NOAA Technical Memorandum ERL SEL-73

OMEGA LONG-TERM PHASE ADVANCES

Herbert H. Sauer
Walther N. Spjeldvik
F. Kenneth Steele

Space Environment Laboratory
Boulder, Colorado
June 1985

noaa NATIONAL OCEANIC AND ATMOSPHERIC ADMINISTRATION / Environmental Research Laboratories

NOAA Technical Memorandum ERL SEL-73

OMEGA LONG-TERM PHASE ADVANCES

Herbert H. Sauer

Walther N. Spjeldvik
Cooperative Institute for Research in Environmental Sciences
Boulder, Colorado

F. Kenneth Steele
National Telecommunications and Information Administration
Boulder, Colorado

Space Environment Laboratory
Boulder, Colorado
June 1985

UNITED STATES
DEPARTMENT OF COMMERCE

Malcolm Baldrige,
Secretary

NATIONAL OCEANIC AND
ATMOSPHERIC ADMINISTRATION

Environmental Research
Laboratories

Vernon E. Derr,
Director

NOTICE

Mention of a commercial company or product does not constitute an endorsement by NOAA Environmental Research Laboratories. Use for publicity or advertising purposes of information from this publication concerning proprietary products or the tests of such products is not authorized.

Contents

List of Figures

OMEGA Long-Term Phase Advances

Herbert H. Sauer

Walther N. Spjeldvik

F. Kenneth Steele

ABSTRACT

Anomalous advances of OMEGA Navigation System 10.2-kHz signals during three extended periods (totaling 60 days) of solar cosmic ray event activity during 1982 are examined and compared with energetic proton, alpha particle, and electron precipitation into the polar cap ionosphere. Time profiles of the OMEGA 10.2-kHz Hawaii-to-Norway path phase advance are found to be almost congruent with the time profiles of the logarithms of the fluxes of energetic protons precipitating into the polar cap as determined from instruments aboard the polar-orbiting NOAA-6 satellite and the GOES-2 geostationary satellite. Although both energetic alpha particles and electrons contribute to the anomalous phase advance experienced by the 10.2-kHz Hawaii-to-Norway OMEGA signal, a simple, empirical algorithm reasonably relates the observed phase advance to the observed differential fluxes of 6-MeV solar cosmic ray protons.

I. INTRODUCTION

It is well known that phase anomalies caused by solar-related changes in the ionospheric reflection heights of Very Low Frequency (VLF) (3-30 kHz) radio waves can impair the positioning capabilities of phase sensitive radio navigation aids such as the OMEGA system (10-14 kHz). Of these anomalies, the sudden phase anomaly (SPA) is probably the most common. It occurs when X-rays emitted during a solar flare ionize the lower ionosphere, causing a rapid phase advance followed by a gradual recovery lasting up to a few hours at VLF. A second phase anomaly, known as the polar cap absorption (PCA) for historical

reasons, is caused by protons emitted during a solar proton event (SPE). The protons are guided by the geomagnetic field into the earth's polar regions where the ionospheric reflection height is lowered, and propagation time can be decreased on a long-term basis (up to 2 weeks) for a single PCA. This report concerns the PCA or long-term phase anomaly, as related to OMEGA signals.

The OMEGA system uses phase-stable signals from eight strategically located 10 kW transmitters (Table 1). Inevitably, transmitters, navigational receivers, or propagation paths will be situated in polar regions where the long-term effects of solar protons may be significant. Swanson (1981) reported that the probability of an OMEGA positioning error of 5 miles or greater is about 0.02 percent for SPA's and nearly 0.2 percent for PCA's. Accordingly, this report presents some recent (1982) phase data that show the effects of propagation in polar regions on OMEGA signals during PCA's and compares these VLF propagation effects with corresponding observations of energetic proton, alpha particle, and electron fluxes precipitating into the high-latitude ionosphere.

The energetic particle measurements were obtained from instrumentation aboard the low-altitude, polar-orbiting NOAA-6 satellite, and comparable instruments aboard the geostationary GOES-2 satellite, both operated by the National Oceanic and Atmospheric Administration (NOAA).

Table 1.--OMEGA Transmitter Locations

OMEGA Station	Location	Latitude	Longitude
A	Norway	66° 25′ 12.39′′ N	13° 08′ 12.65′′ E
B	Liberia	6° 18′ 19.39′′ N	10° 39′ 44.21′′ W
C	Hawaii, USA	21° 24′ 16.9 ′′ N	157° 49′ 52.7 ′′ W
D	North Dakota, USA	46° 21′ 57.2 ′′ N	98° 20′ 8.77′′ W
E	Reunion Is., FR	20° 58′ 26.47′′ S	55° 17′ 24.25′′ E
F	Argentina	43° 03′ 12.53′′ S	65° 11′ 27.69′′ W
G	Australia	38° 28′ 52.68′′ S	146° 56′ 6.36′′ E
H	Japan	34° 36′ 53.26′′ N	129° 27′ 12.49′′ E

This report has three purposes:

1) To compare the time histories of the fluxes of protons, alpha particles, and electrons precipitating into the high-latitude ionosphere with the corresponding phase advance observed in the OMEGA VLF signals.

2) To evaluate the relative contributions of the several particle fluxes to the increased ion-pair production rate in the ionosphere.

3) To examine the results of these comparisons for evidence of additional or contributing mechanisms that might operate to enhance or prolong the PCA phase anomalies observed on the OMEGA signals.

II. SELECTION OF DATA PERIODS

1. INTRODUCTION

There is a large body of literature and data pertinent to the effects of radiation or particles on VLF/OMEGA signals. For purposes of this report, the most desirable data show the phases of the basic OMEGA navigation signals (10.2 kHz) that propagate through polar regions. Fortunately (Morris, 1983, private communication), the OMEGA system routinely monitors the phases of its 10.2-kHz signals that are transmitted on a sequenced schedule from each of the eight transmitters. The highly coherent phase monitoring is performed at sites that are often at or near OMEGA transmitters. The great-circle propagation paths between these transmitters are sometimes transpolar and can be the sources of useful propagation data. For example, the geometrically reciprocal paths between Hawaii and Norway (10,208 km), and the path from Australia to Argentina (10,386 km) are transpolar. The North Dakota-to-Hawaii path (5,988 km) is in middle latitudes and can be used for comparisons. Phase monitoring of these paths was essentially continuous during much of 1982 when there were interesting and significant effects of solar activity.

Probable solar proton effects on OMEGA signals may be identified with the knowledge that the PCA is typically preceded by a large SPA, and is seen as a phase advance that lasts from 5 to 15 days at VLF (Davies, 1965).

2. DETERMINATION OF ANOMALOUS PHASE

The observed phases of VLF radio signals received over long paths show the combined effects of regular diurnal and seasonal variations in solar illumination and some anomalous effects due to solar X-rays and solar protons (Davies, 1965). Recently, galactic X-rays have been suggested as a cause of some anomalous VLF phase behavior also (Chilton and Crary, 1971; Piazza et al., 1983).

To isolate the anomalous phase it is necessary to remove the normal or characteristic phase from the observed phase. The normal or 'quiet' day phase is obtained during periods when no SPA's are observed and when the phase returns to the same approximate value each day or night at any given time. At the higher frequencies within the VLF band, the phase may not return to the phase level of the preceding day because of modal interference (Crombie, 1964). At OMEGA frequencies, however, especially at 10.2 kHz, the phase is particularly stable both by day and by night. An average of a few normal days immediately preceding or following a suspected event will establish a datum level for quantifying anomalous phase; i.e., anomalous phase is the difference between observed phase and the average of normal days. Although there is a small seasonal change in received normal phase during the period of a given PCA, it is considered to be negligible compared with the anomalous phase.

The phases of the 10.2-kHz signals from Hawaii as received in Norway on five quiet days in January 1982 were sampled hourly, averaged, and plotted (Figure 1). The received phase of these signals, sampled hourly on 30 and 31 January is shown for comparison. It is readily apparent that the observed phase begins to depart from the quiet-day average at about 0500 UT on 30

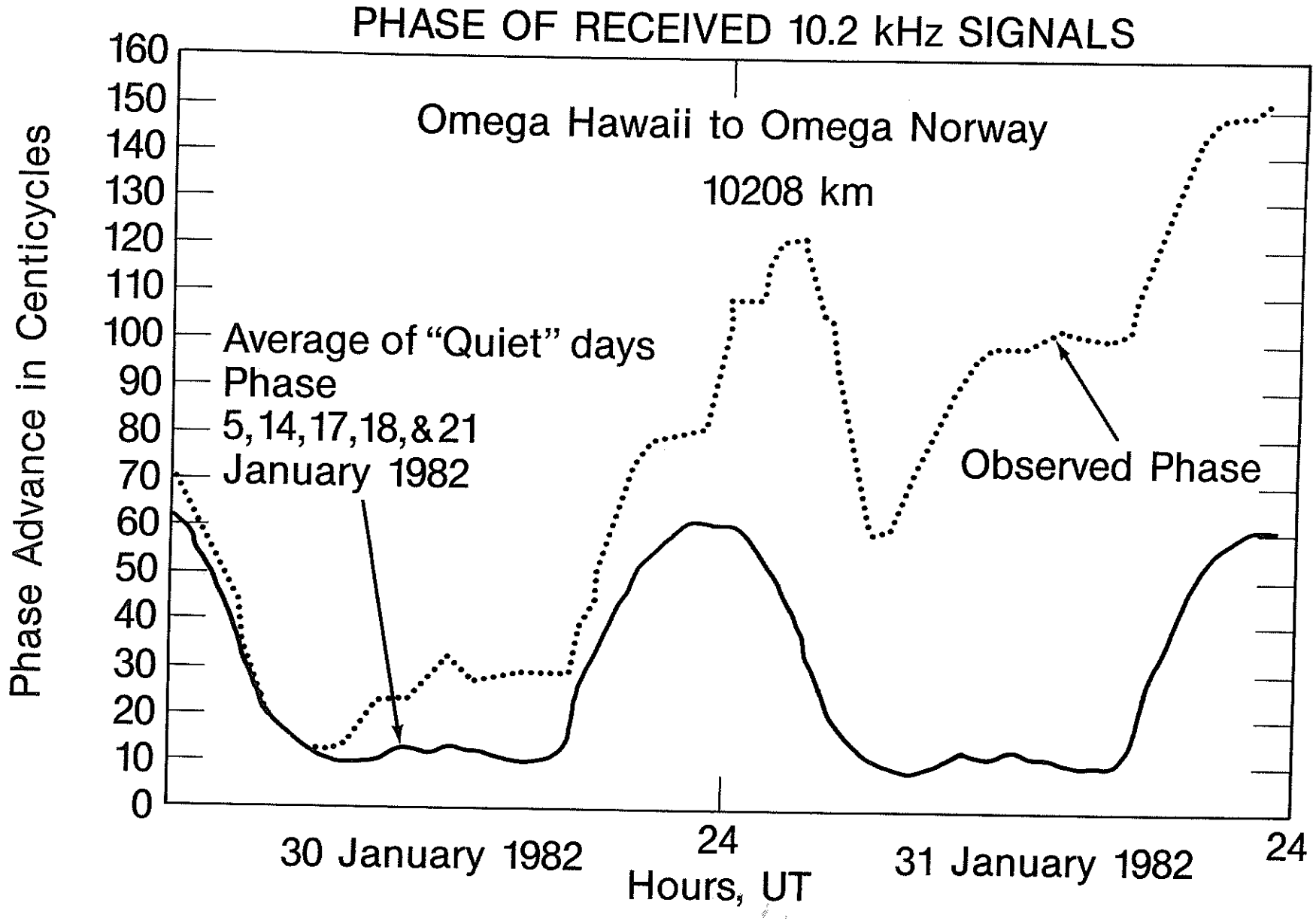

Figure 1 Comparison of Observed and Quiet Day Phase Advance

January and reaches a maximum departure of about 95 centicycles at 2300 UT on 31 January.

3. EVENT PERIODS

OMEGA phase data taken at 10.2 kHz in Hawaii, Norway, and Argentina in 1982 were examined and some periods suggestive of solar proton activity were identified. Quiet-day averages for these periods were removed from the observed phase to obtain the anomalous phase. Some typical results, which have been photographically reduced to tractable size, are shown in Figures 2, 3, and 4.

Figure 2 shows the anomalous phases of the 10.2-kHz signals from Hawaii as observed in Norway from 30 January to 12 February 1982. A gradual phase advance begins about 0500 UT on 30 January, followed by a large SPA at 2300 UT on the same day. After recovery from the SPA, the phase continues to advance to a maximum of nearly 85 centicycles at 2300 UT on 31 January. Thereafter, there is a gradual return toward normal phase until 6 February. On that day, there is a small phase advance, which lingers for 2 days. The phase then gradually returns to normal on 12 February.

For comparison, Figure 3 shows the phases of 10.2-kHz signals received over auroral, austral, and middle-latitude propagation paths during the period 11 through 25 July 1982. The phases of signals propagating through both polar regions show similar characteristics. The phases advance to about 80 to 85 centicycles at nearly the same time and gradually recover until late on 22 July when a second event occurs, followed by a recovery period. There is an

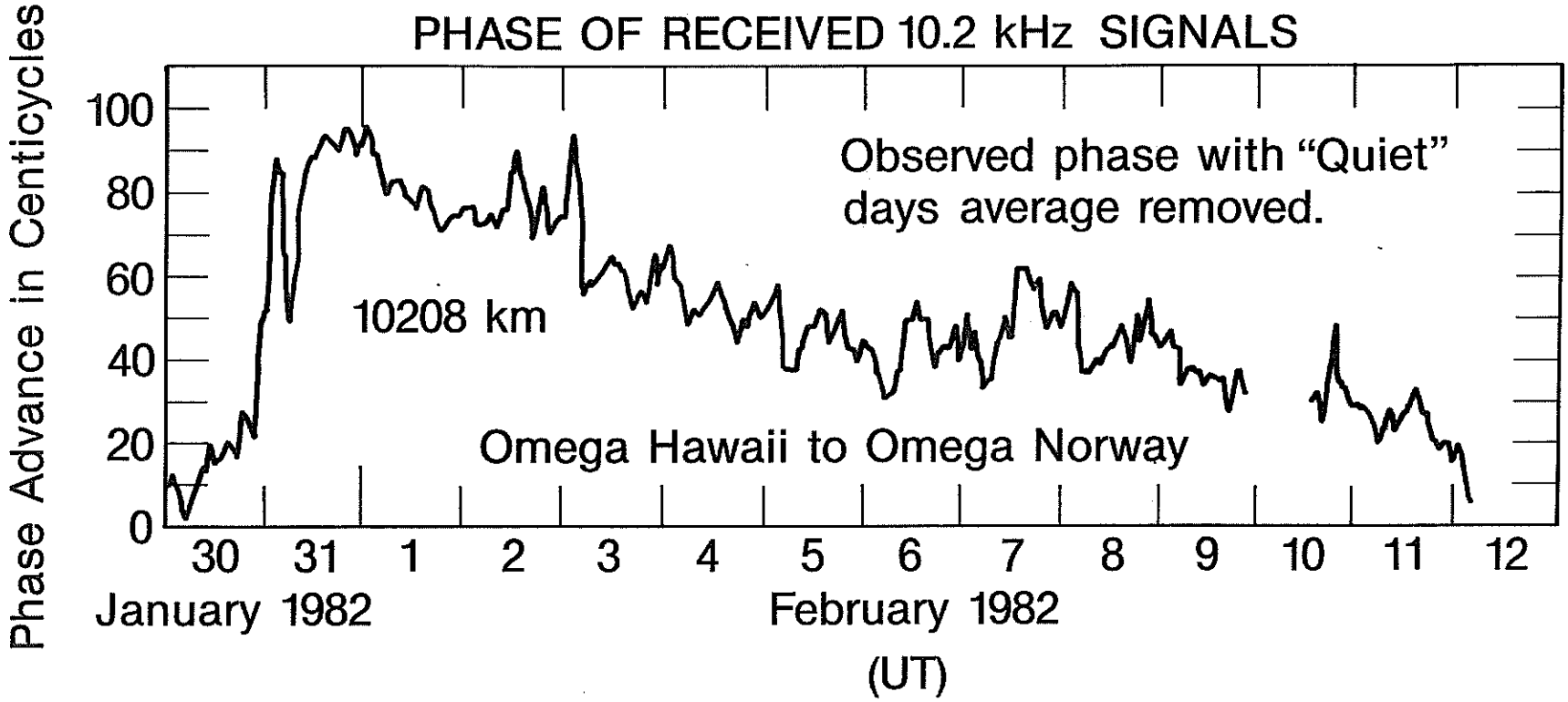

Figure 2 Hawaii-Norway Phase Advance 30 January - 12 February, 1982.

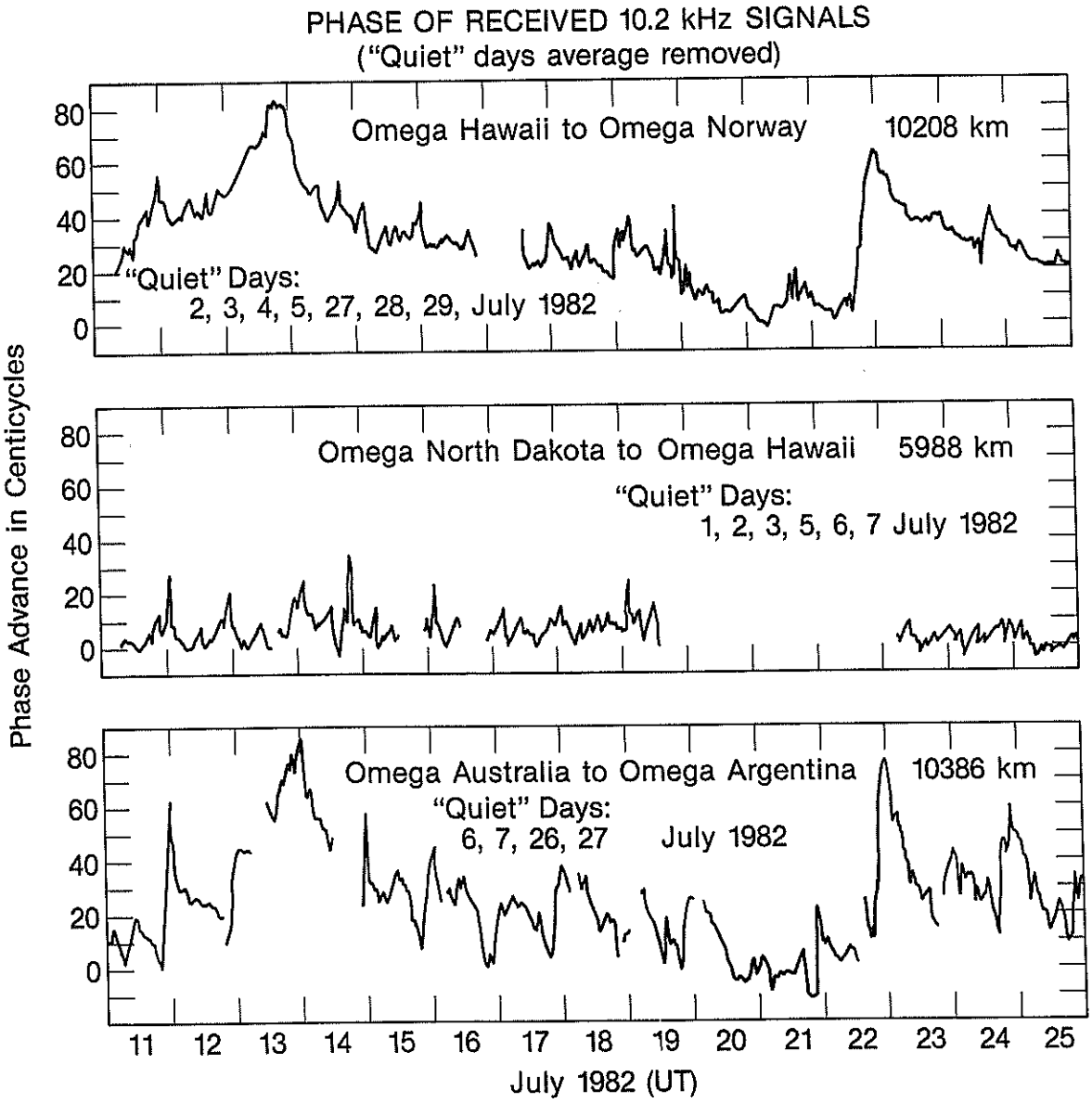

Figure 3 Observed Phase Advances 11 July - 25 July, 1982

greater phase variability on the southern path. This is probably due to a weak transmitted signal from Australia at that time (Morris, 1983, private communication). The phase of the signals from North Dakota received over the middle-latitude path to Hawaii show no large long-term variations like those on the polar paths. This is expected since the geomagnetic field at lower latitudes prevents charged solar particles from penetrating into the lower ionosphere. At high latitudes, however, the ionizing particles encounter lower retarding force from the geomagnetic field. The absence of a long-term phase anomaly on the middle-latitude path strongly suggests then that during these disturbances the high latitude paths are ionized solely by charged particles. The anomalous phase of the 10.2-kHz transmissions from Norway as received in Hawaii from 7 through 15 December 1982 is shown in Figure 4. The phase advanced very rapidly on 8 December, and reached a maximum of nearly 85 centicycles at about 0430 UT on the same day. There was a rapid partial recovery of phase followed by a gradual one beginning at 00 UT on 9 December and lasting until 15 December.

4. REMARKS

Three periods of anomalous phase, typical of those associated with solar proton activity, have been identified and presented. They last from 8 to 14 days. As might be expected, only high-latitude propagation paths showed the effects of suspected solar proton activity. Since a middle-latitude path shows no long-term phase anomaly, it seems unlikely that galactic X-rays could have contributed to the phase anomalies observed on the polar paths at that time.

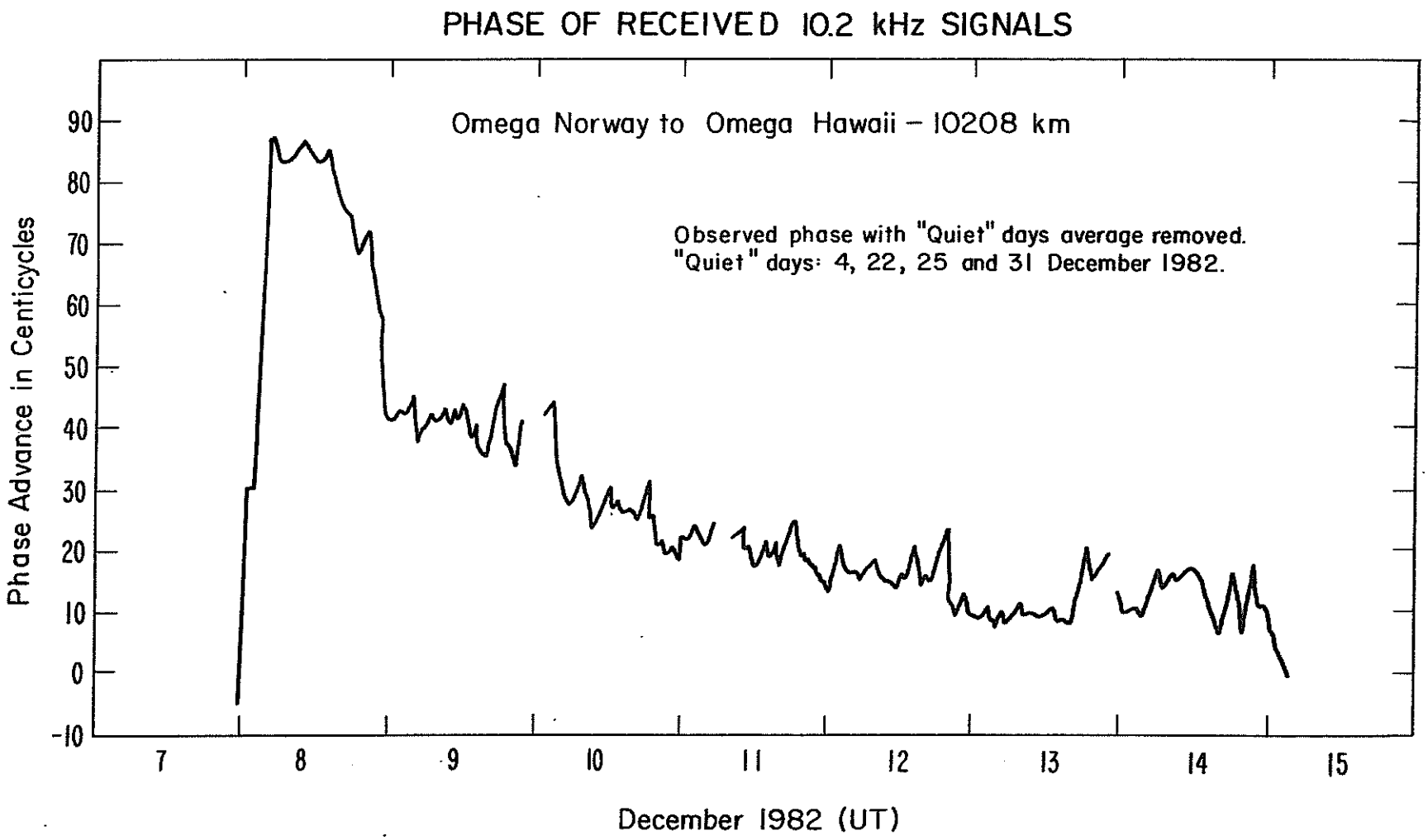

Figure 4 Norway - Hawaii Phase Advance 7 December - 15 December, 1982

The following sections will present and discuss the corresponding observations of energetic particle precipitation into the high-latitude ionosphere.

III. PARTICLE DATA SOURCES

1. INTRODUCTION

The NOAA Space Environment Laboratory maintains space environment monitors aboard the TIROS series of low-altitude, sun-synchronous, polar-orbiting satellites, and aboard the SMS/GOES series of satellites operating in geostationary orbit. The particle data used in this study were obtained from the Energetic Particle Sensors (EPS) aboard the NOAA-6 satellite of the TIROS series, and from the Space Environment Monitor (SEM) aboard the GOES-2 satellite of the SMS/GOES series. Although the GOES SEM does not directly measure the cosmic ray fluxes incident in the high-latitude or polar cap regions, the geomagnetic cutoff operating at geostationary orbit is quite low (typically less then 5 MeV), and therefore observations at geostationary orbit are representative of those in the polar cap after the initial (several hours) anisotropic phase of a solar cosmic ray event. It is also during the initial anisotropic phase that impact zone effects (Firor, 1954) prevent even the polar cap from being uniformly illuminated by the solar cosmic rays.

2. THE NOAA-6 ENERGETIC PARTICLE SENSOR

The TIROS-NOAA series of satellites are three-axis stabilized and are in sun-synchronous, 98° inclination, 850-km-altitude circular orbits. The local time of the satellite orbital plane varies from satellite to satellite, being 0730 and 1930 hours local time for NOAA-6. The instrumentation on board each satellite of the series includes an Energetic Particle Sensor (EPS) to measure

the charged particle population over a wide range of energies. The EPS consists of two sensor subassemblies; the MEPED (Medium Energy Proton and Electron Detector), and the Omnidirectional or Dome detectors.

A. MEPED - MEDIUM ENERGY PROTON AND ELECTRON DETECTOR

The MEPED consists of four sensors a pair of which view the local zenith (precipitating particles), and a pair that 'look' at approximately 90° to the zenith (locally mirroring or trapped particles). Each pair consists of a proton telescope and an electron detector.

The proton telescope (Fig. 5) has a geometric factor of 9.5×10^{-3} cm-ster. Electrons are eliminated with a 2.5-kilogauss (minimum field strength) Alnico VIII Magnet. No particle with a magnetic rigidity of less than 6200 gauss-cm can strike the detector unless it scatters. This threshold corresponds to 1.5 MeV for electrons and 2 keV for protons. The proton threshold for the telescope is $\simeq$ 30 keV. These ions have a radius of curvature greater than 40 cm in the field of the magnet, and should therefore be virtually unaffected by the presence of the magnetic field of the magnet. The telescope consists of 2- μm-thick silicon surface barrier detectors. The front detector (D1) has an effective area of 25 mm^2; the second detector (D2) has an effective area of 50 mm^2.

Each proton telescope measures ions in six energy passbands over the range of 30 keV to > 2.5 MeV through the application of selective logic on the detector discrimination levels. For the purpose of this study, only the > 2.5-MeV measurements of the detector were used.

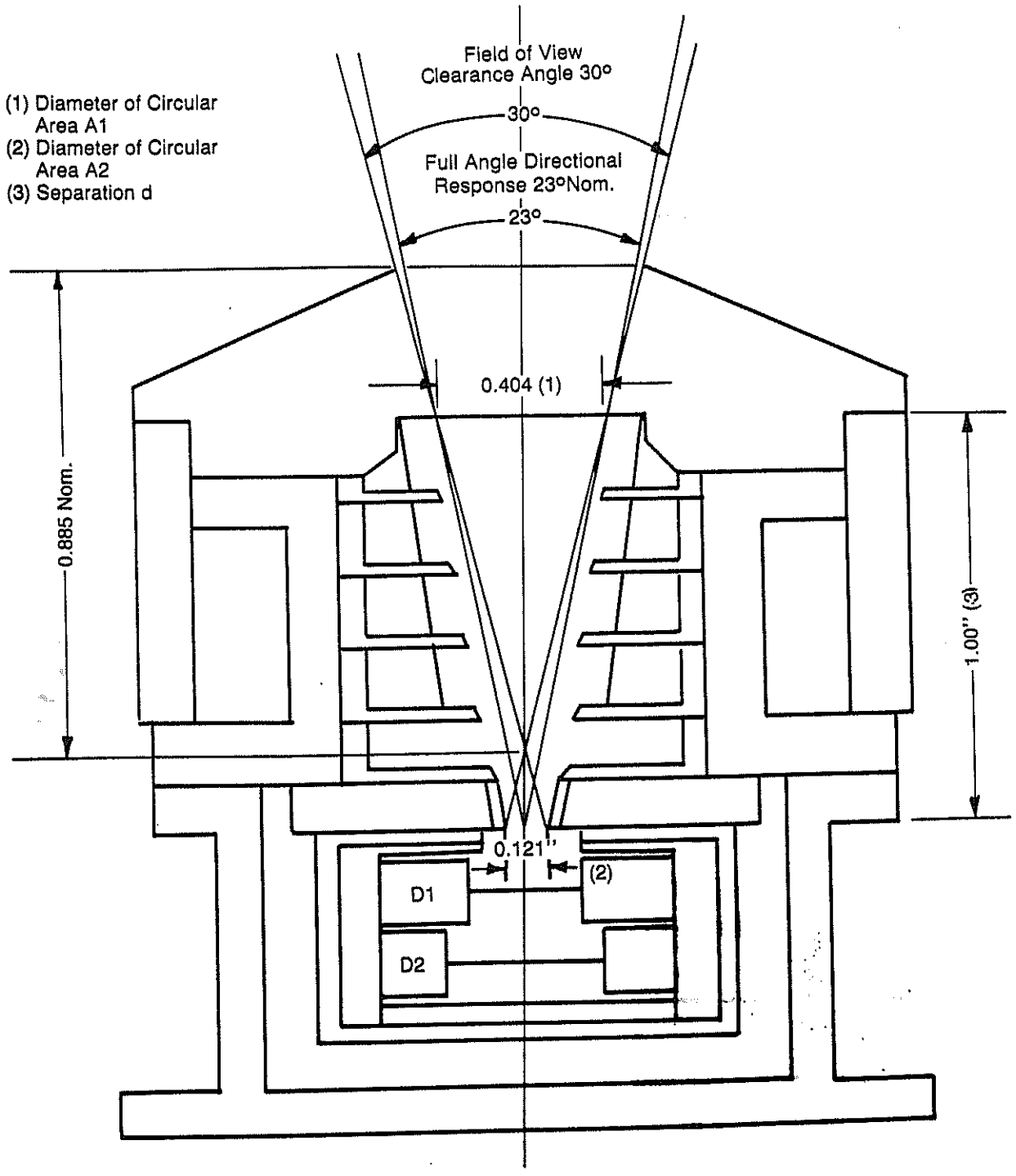

Figure 5 NOAA EPS Proton Telescope

The electron detector (Figure 6) has the same geometric factor as the proton telescope, 9.5×10^{-3} cm^2-ster. The detector is a 1700-μm-thick, 25-mm^2 silicon surface barrier, and the system incorporates a thin nickel foil in front of the aperture to reduce the proton contribution to the detector count rate. The foil is approximately 20 μm thick, and removes any sensitivity to protons below 175 keV. Anti-coincidence logic effectively removes any proton sensitivity above about 1.1 MeV from the electron detector.

B. The Dome Detector

The Dome or omnidirectional sensors (Fig. 7) are essentially identical to the unit flown on the GOES-2 spacecraft, and comprise three nominally identical Kevex, lithium-drifted, silicon solid-state detectors 0.50 cm square and 3 mm thick. They are independently mounted under spherical shell moderators to provide sensitivity in three integral data channels. Each detector has a full viewing angle of 120° in the zenithal direction as mounted on the spacecraft. The overall out-of-aperture shielding of each detector is identical, at 80 MeV, in order that the principal spurious response may be eliminated through simple subtraction of the appropriate detector count rates.

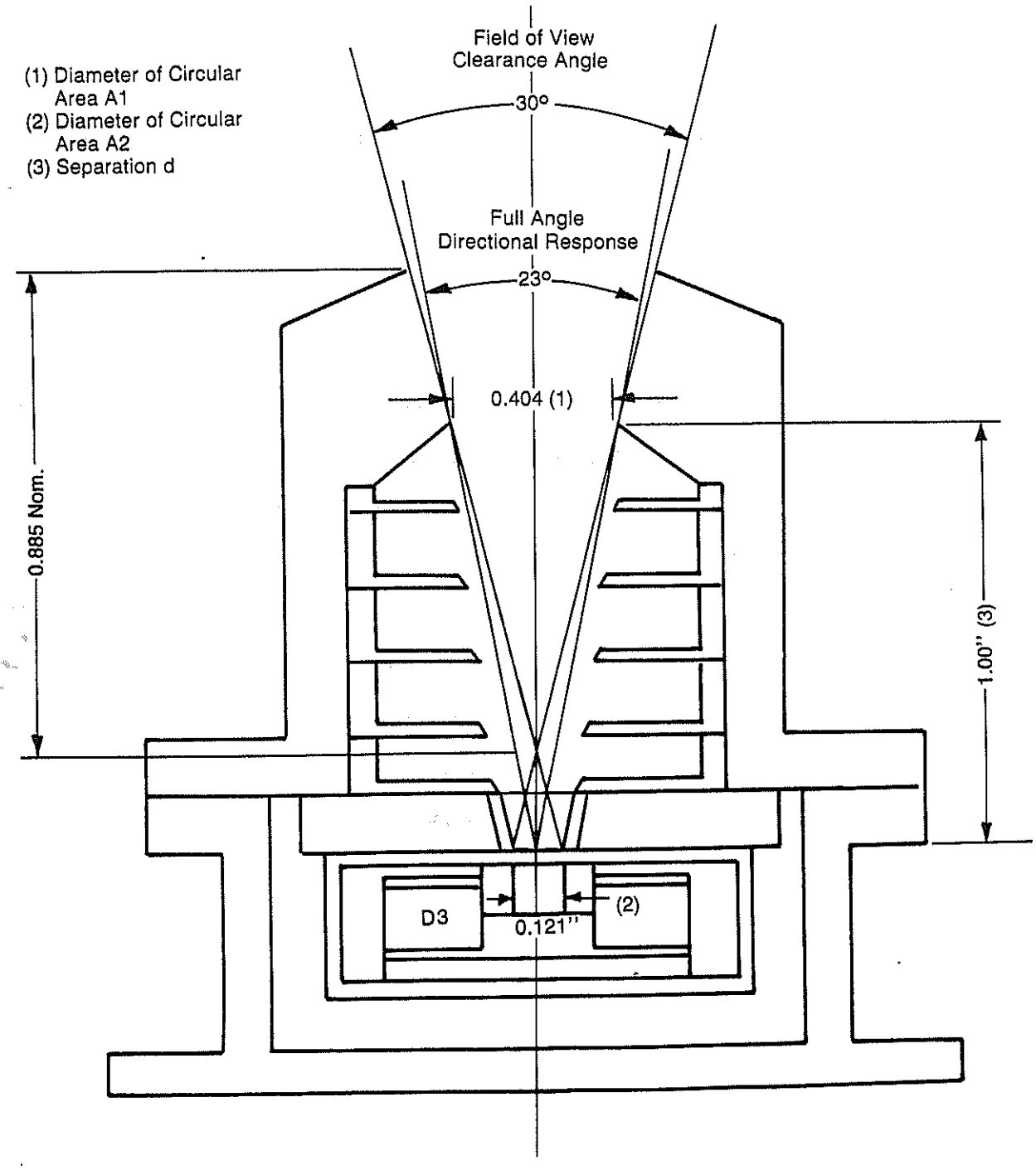

Figure 6 NOAA EPS Electron Telescope

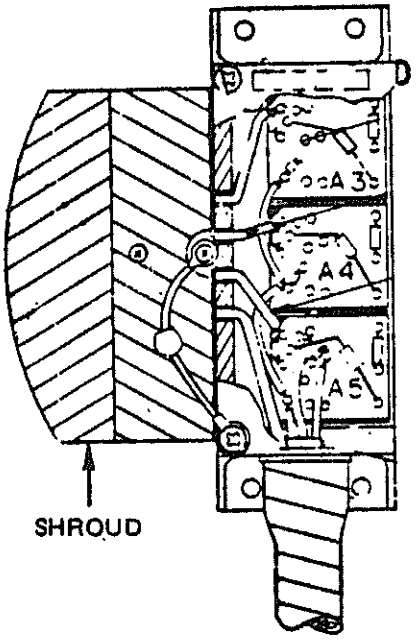

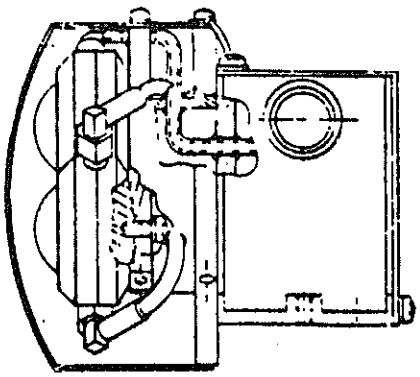

D3 ALUMINUM DOME
D4 COPPER DOME
D5 TUNGSTEN DOME

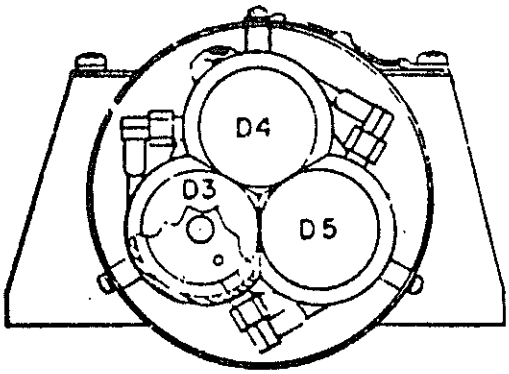

"KEVEX"
Si (Li)
DETECTOR 3 PLACES

Figure 7 NOAA EPS Dome Detector

C. NOAA-EPS Characteristics

The pertinent characteristics of the EPS detectors appropriate to this study are given in Table 2.

TABLE 2.--NOAA-EPS characteristics

Ion	Channel designation	Energy	Geometric factor (cm^2 ster)	Accumulation time (s)
Proton	P1	>2.5 MeV	9.4×10^{-3}	1
Proton	P2	16-80 MeV 80-215 MeV	1.57 5.4	2
Proton	P3	36-80 MeV 80-215 MeV	1.57 5.4	2
Proton	P4	80-215 MeV	5.4	2
Electron	E1	>30 keV	9.5×10^{-3}	1
Electron	E2	>100 keV	9.5×10^{-3}	1
Electron	E3	>300 keV	9.5×10^{-3}	1

3. The GOES-2 Energetic Particle Sensor

The NOAA Space Environment Laboratory maintains Space Environment Monitors (SEM) aboard the SMS/GOES series of meteorological satellites operating in geostationary orbit. The SEM instruments measure the flux of solar X-rays reaching the earth from the sun, the populations of energetic electrons, protons, and alpha particles, and the direction and magnitude of the geomagnetic field at the (geostationary) satellite. These data provide a principal real-time system in support of the laboratory mission of providing continued monitoring of the geophysical environment, and forecasts and

warnings of geophysical disturbances.

A. The Low-Energy Telescope

Spectral analysis of protons and alpha particles is accomplished using two independent particle sensors. A narrow-aperture telescope responds to low-energy particles: protons of energy 0.8 to 15 MeV, and alpha particles of energy 3.2 to 60 MeV. A wide-angle spectrometer responds to high-energy particles: protons of energy 17.0 to 500 MeV, and alpha particles of energy 70.0 to 412 MeV. The analog signals from the sensors are processed according to energy and particle species, and accumulated in the appropriate particle counters.

A cross section of the GOES low-energy-telescope is shown in Figure 8. The sensor consists of two 55- μm thick silicon detectors of 100 mm^2 area. Care has been exercised to ensure that the telescope collimators prevent energetic particles that penetrate the upper detector from missing the lower detector, thereby decreasing contamination of the observed low-energy particle spectra by out-of-aperture penetrating particles. A thin (2 μm) aluminum foil covers the telescope entrance aperture, to provide a light shield to the detector system.

B. The Dome Detector

As noted previously, the Dome detectors of the EPS aboard the NOAA-6 and GOES-2 spacecraft are nominally identical, and the reader is therefore referred to sect. 2.B for their description.

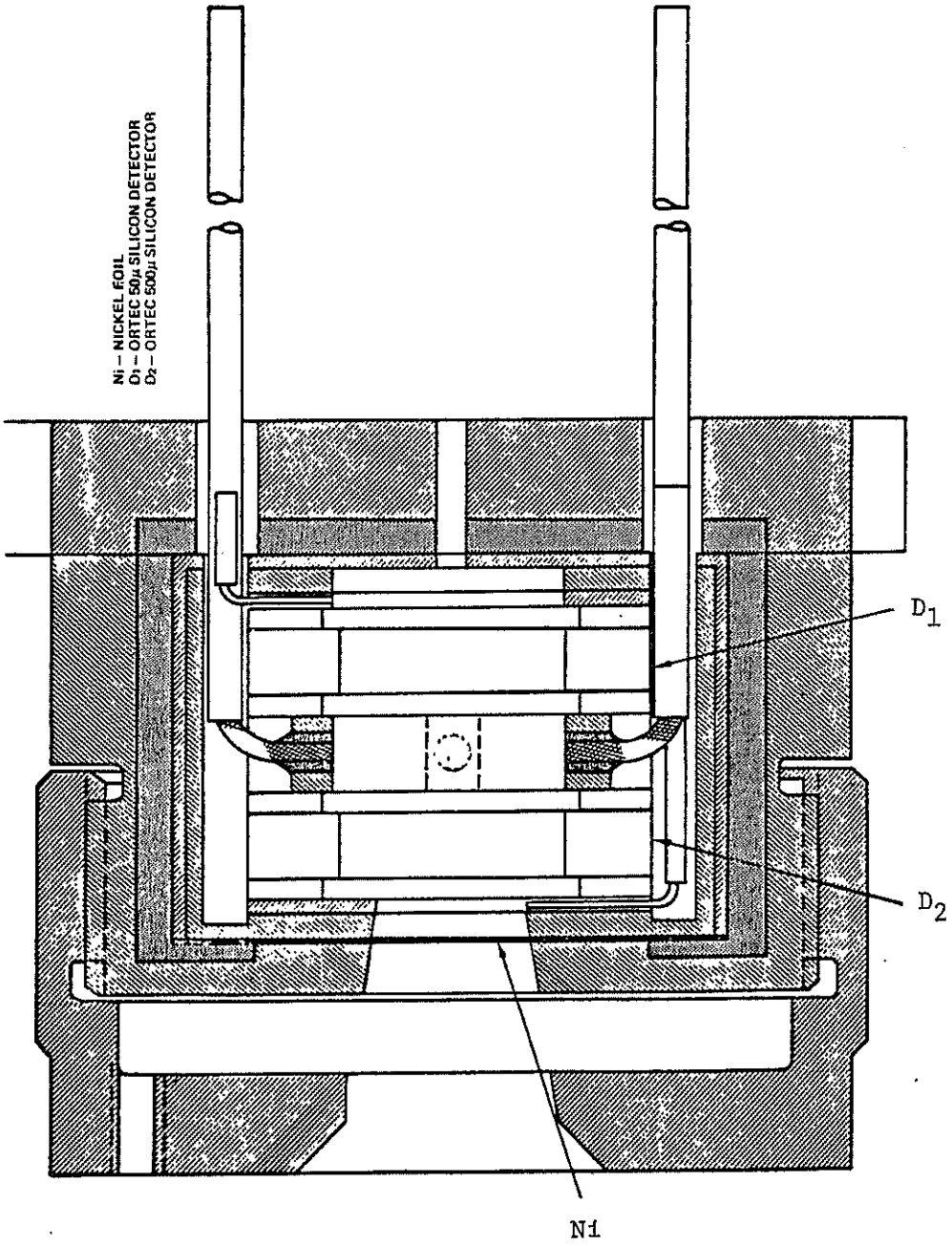

Figure 8 GOES EPS Low Energy Telescope

C. GOES EPS Characteristics

The pertinent characteristics of the GOES-2 EPS detectors appropriate to this study are given in Table 3.

Table 3.--GOES EPS characteristics

Ion	Channel designation	Energy	Geometric factor (cm^2 ster)	Accumulation time (s)
Proton	P1	4-8 MeV	0.14	12.3
Proton	P2	8-16 MeV	0.14	12.3
Proton	P3	36-80 MeV	1.57	12.3
		80-215 MeV	5.4	
Proton	P4	80-215 MeV	5.4	6.14
Alpha	A1	3.2-10 MeV	0.35	12.3
Alpha	A2	10-16 MeV	0.14	12.3
Alpha	A3	16-20 MeV	0.14	12.3
Alpha	A4	85-182 MeV	1.57	12.3

4. DATA COMPARISONS AND ANALYSIS

Because of the shielding effect of the geomagnetic field, which becomes more pronounced at lower geomagnetic latitudes or L-values, charged particles of a given energy may penetrate the geomagnetic field to the earth (properly, the top of the atmosphere) only above a specific latitude λ_c, the cutoff latitude. The minimum energy corresponding to this cutoff latitude is termed the cutoff energy (see Rossi & Olbert, 1979). Further, for a static geomagnetic field, Liouville's Theorem asserts that the directional flux of particles along an allowed particle trajectory is conserved, or constant. If the flux of, say, solar cosmic ray particles is uniform and isotropic outside the earth's magnetosphere, then Liouville's Theorem assures that the flux measurements made at two distinct locations on the earth will yield the same

result if the particle energies observed are above local cutoff. Although interplanetary fluxes of solar cosmic rays are often found to be anisotropic during the early (some several hours) phases of an event, they generally remain sensibly isotropic and uniform for the remaining hours to days of that event.

The cutoff energy for protons and alpha particles at geostationary orbit are seldom above a few MeV (Lanzerotti, 1968), and therefore one can estimate that, at least after any initial anisotropic phase, the fluxes of particles above several MeV as measured at geostationary orbit are representative of those that would be observed over the polar caps where the geomagnetic cutoff is sensibly zero. Further confidence in this assumption is obtainable for the present measurements in that proton fluxes are measured both at geostationary orbit by detectors aboard the GOES-2 satellite, and at high latitudes by corresponding detectors aboard the NOAA-6 satellite. The fact that the proton fluxes so measured at geostationary orbit and at high latitude agree to good accuracy for all the event periods studied for this report, serves to validate the use of the geostationary alpha particle observations to represent those that would be observed over the polar caps.

A. DATA COMPARISONS

The following pages present comparisons of the energetic proton, alpha, and electron fluxes precipitating into the polar ionosphere and the phase advance of the 10.2-kHz OMEGA signal observed on the Hawaii-Norway (H-N) path. The three extended periods during 1982 that are examined encompass some seven episodes of solar cosmic ray events in which the observed phase advance exceeded 40 centicycles (see Table 4).

Table 4--Approximate peak event times

Data period	Approx. peak UT time	Day	Peak Hawaii-Norway 10.8-kHz phase advance (centicycle)
Day 30-44	0100	31	85
Day 192-213	1600	194	87
	0400	204	64
Day 340-366	1000	342	88
	1300	351	45
	0100	354	47
	1400	361	64

A table of the correspondence between day of the year number (Jan. 1 = Day 1) and calendar date is given in the Appendix.

Note that particle data obtained from the NOAA-6 satellite are obtained in integral flux units, whereas those obtained from the GOES-2 satellite are given in differential flux units. Table 5 gives the energy ranges and particle species denoted by the channel designations for each satellite data set in this report.

Table 5--Data channel characteristics

GOES-2			NOAA-6		
Channel	Species	Mean Energy	Channel	Species	Energy
A1	Alpha	6.6 MeV	E1	Electron	> 30 keV
A2	Alpha	13.0 MeV	E2	Electron	>100 keV
A3	Alpha	18.0 MeV	E3	Electron	>300 keV
A4	Alpha	132.0 MeV			
P1	Proton	6.0 MeV	P1	Proton	>2.5 MeV
P2	Proton	12.0 MeV	P2	Proton	> 16 MeV
P3	Proton	58.0 MeV	P3	Proton	> 36 MeV
P4	Proton	145.0 MeV	P4	Proton	> 80 MeV

Figure 9 presents plots of the particle fluxes observed with the NOAA-6 and GOES-2 particle detectors, together with the 10.2-kHz phase advance observed on the Hawaii-Norway (H-N) path for the first event period extending from Day 30 (Jan. 30) through Day 43 (Feb. 12). Each particle data trace is identified with the appropriate channel designation, as well as with the scale factor applied to that data channel in order that the traces be well separated on the plots.

For this period, there was a data outage on both the NOAA and GOES data sets as indicated by the gaps in the traces of Figure 9. However, it is evident that the time history of the H-N phase advance tracks the P1 fluxes of both the GOES and TIROS data quite well, except that the GOES P1 trace essentially dropped to background levels ($< 10^{-1}/cm^2 sec\ ster\ MeV$) by the end of Day 40, while the H-N phase advance was still ~25 centicycles, not fully recovering until the end of Day 42. The alpha particle fluxes are seen to

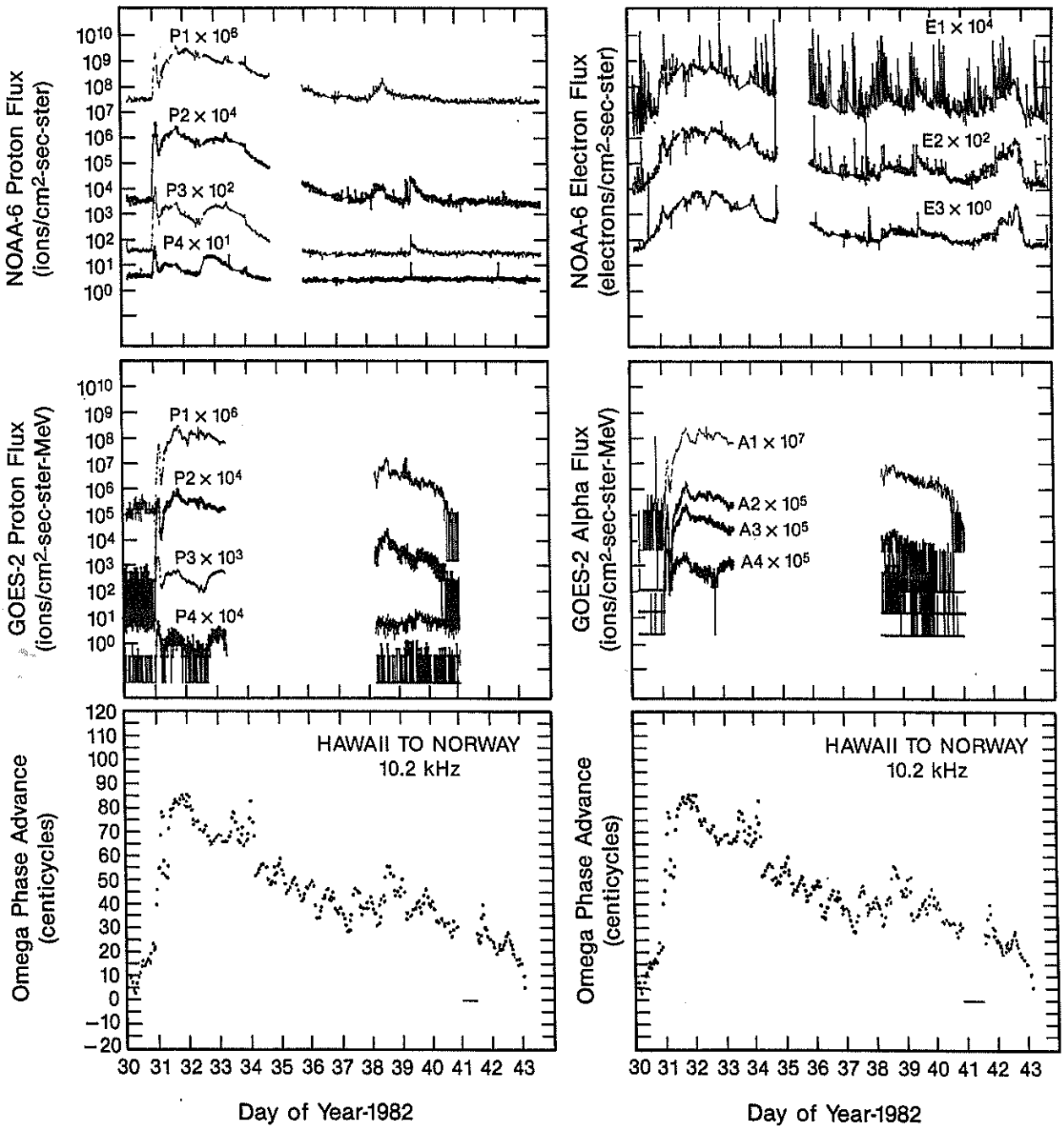

Figure 9 Comparison of Particle Fluxes with
30 January - 12 February, 1982

have a time profile very similar to that of the protons (i.e., the alpha-proton ratio remained quite constant throughout the event), but the electron fluxes showed a period of substantial increase during Day 42. However, the apparent delayed recovery of the H-N phase advance can probably not be attributed to the monotonic increase of electron fluxes during Days 41 and 42, since the H-N phase advance continues decreasing to zero through the same period.

In the same format, Figure 10 presents the time profiles of the NOAA and GOES proton fluxes and the anomalous phase advance observed on the H-N path, for the period from Day 192 (11 July) through Day 212 (31 July). Figure 11 shows the corresponding electron and alpha particle observations during the same period. This data period encompasses two distinct solar cosmic ray events peaking at approximately the start of Day 195 (14 July) and Day 204 (23 July). The high degree of similarity between the profiles of the H-N phase advance and the proton and alpha fluxes is evident throughout the 20 day period. There is essentially no evidence in either event of delayed recovery of the OMEGA signal. Again, looking primarily at the GOES P1 channel, both the H-N phase and the 6 MeV proton fluxes shown by the P1 channel recover at approximately the same time at the end of Days 202 and 207, respectively. For this event period as well, the alpha-proton ratio remained quite constant, as indicated by the similarity between the profiles of the observed alpha particles (Fig. 11), and protons shown in Figure 10. During these two midsummer events, the H-N path would have been almost continuously sunlit, and one would expect to see little effect of the dependence of anomalous phase advance on the fraction of sunlit path noted by Argo (1975).

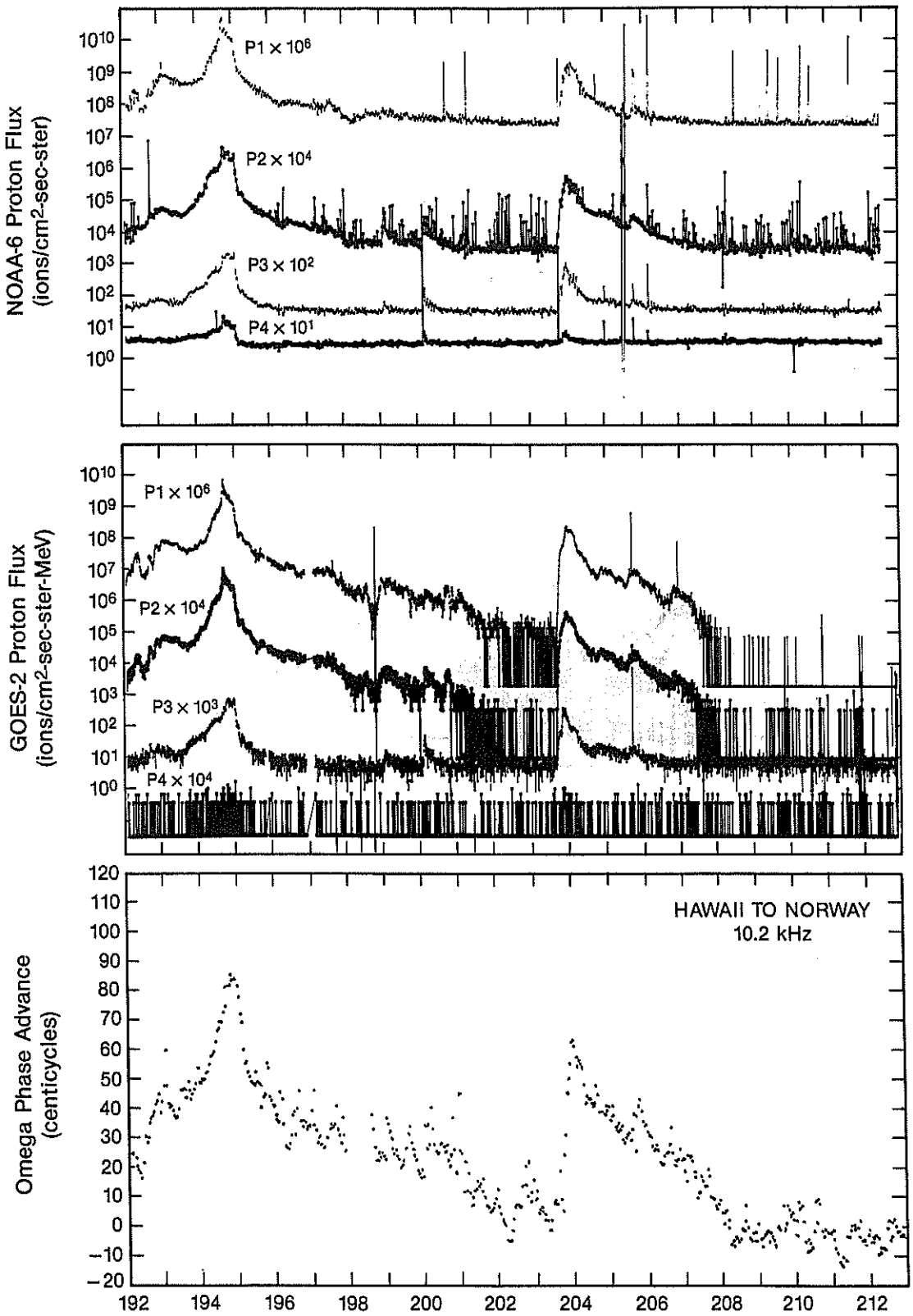

Figure 10 Comparison of Proton Fluxes with H-N Phase Advance 11 July - 31 July, 1982

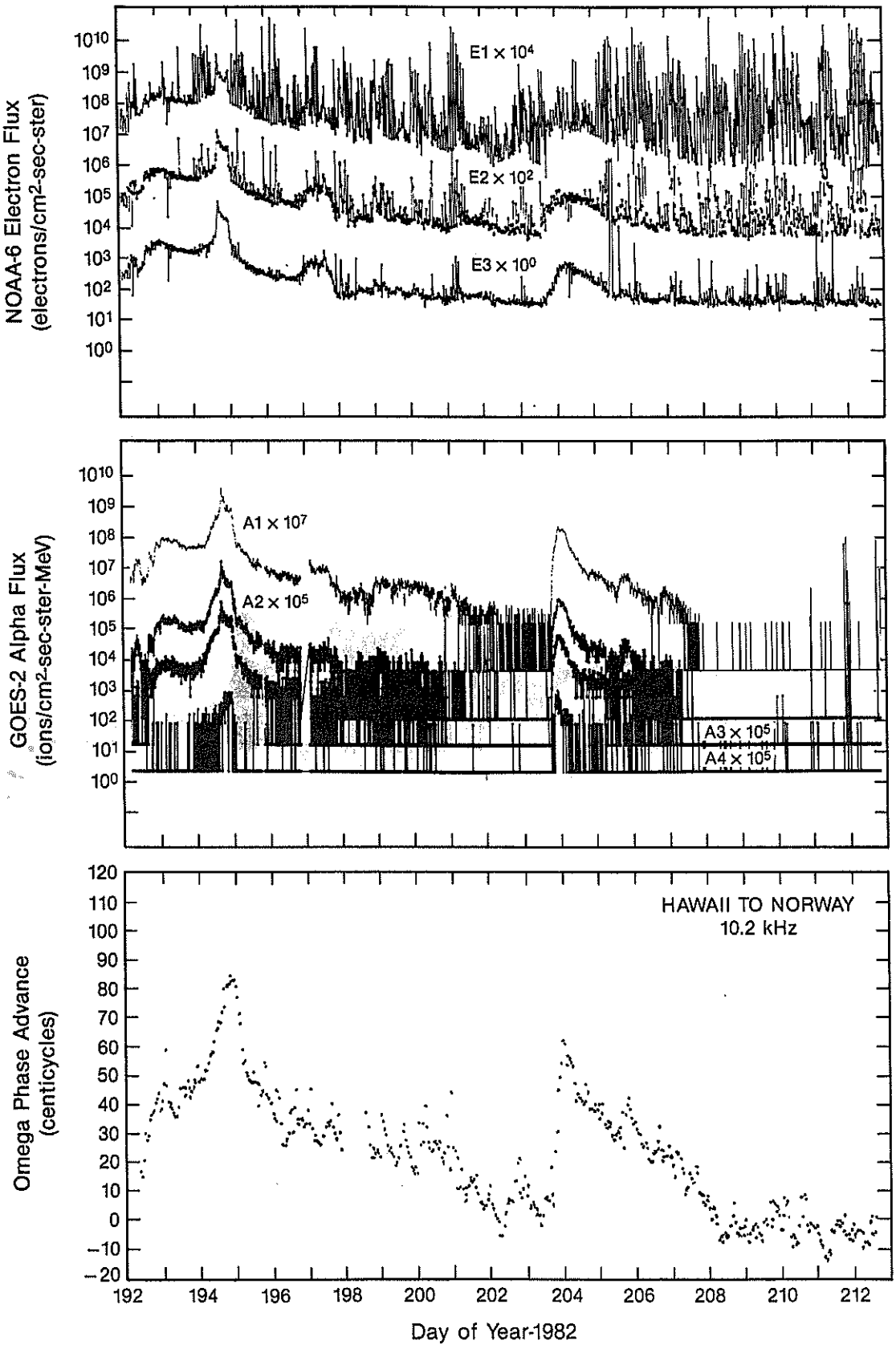

Figure 11 Comparison of Alpha Particle and Electron Fluxes with H-N Phase Advance 11 July - 31 July, 1982

Finally, Figures 12 and 13 show the corresponding data comparison for the event period running from Day 340 (6 Dec.) through Day 365 (31 Dec.). During this period, there were several solar cosmic ray events with the H-N anomalous phase (and corresponding particle fluxes), showing relative maxima early on Day 342 (8 Dec.), on Day 352 (18 Dec.), on Day 354 (20 Dec.), and early on Day 361 (27 Dec.). Again, the time profiles of both the proton and alpha particle fluxes show a high degree of similarity to the profile of the H-N anomalous phase during the entire 26 day period encompassing the four solar cosmic ray event maxima. Throughout this period, there is no evidence for delayed recovery of the H-N anomalous phase with respect to the 6 MeV (P1) proton flux observations of the GOES satellite. Although significant electron precipitation fluxes have accompanied all solar cosmic ray events, their time profiles do not at all show the same high degree of similarity to the profile of the H-N anomalous phase as that shown by the proton and alpha particle fluxes.

B. ION PRODUCTION

Calculations have been made of the ionospheric ion production rates due to each particle species observed by the NOAA-6 and GOES-2 satellites at both the approximate time of the peak of the anomalous phase advance of the H-N signals, and late in the event for seven solar cosmic ray event periods. Estimates of the resulting electron density profiles have also been made using the empirical ionospheric steady-state coefficients given by Adams and Masley (1965). The ion production rates due to the observed proton and alpha particle fluxes were calculated using a computer code generously provided by G. W. Adams (private communication).

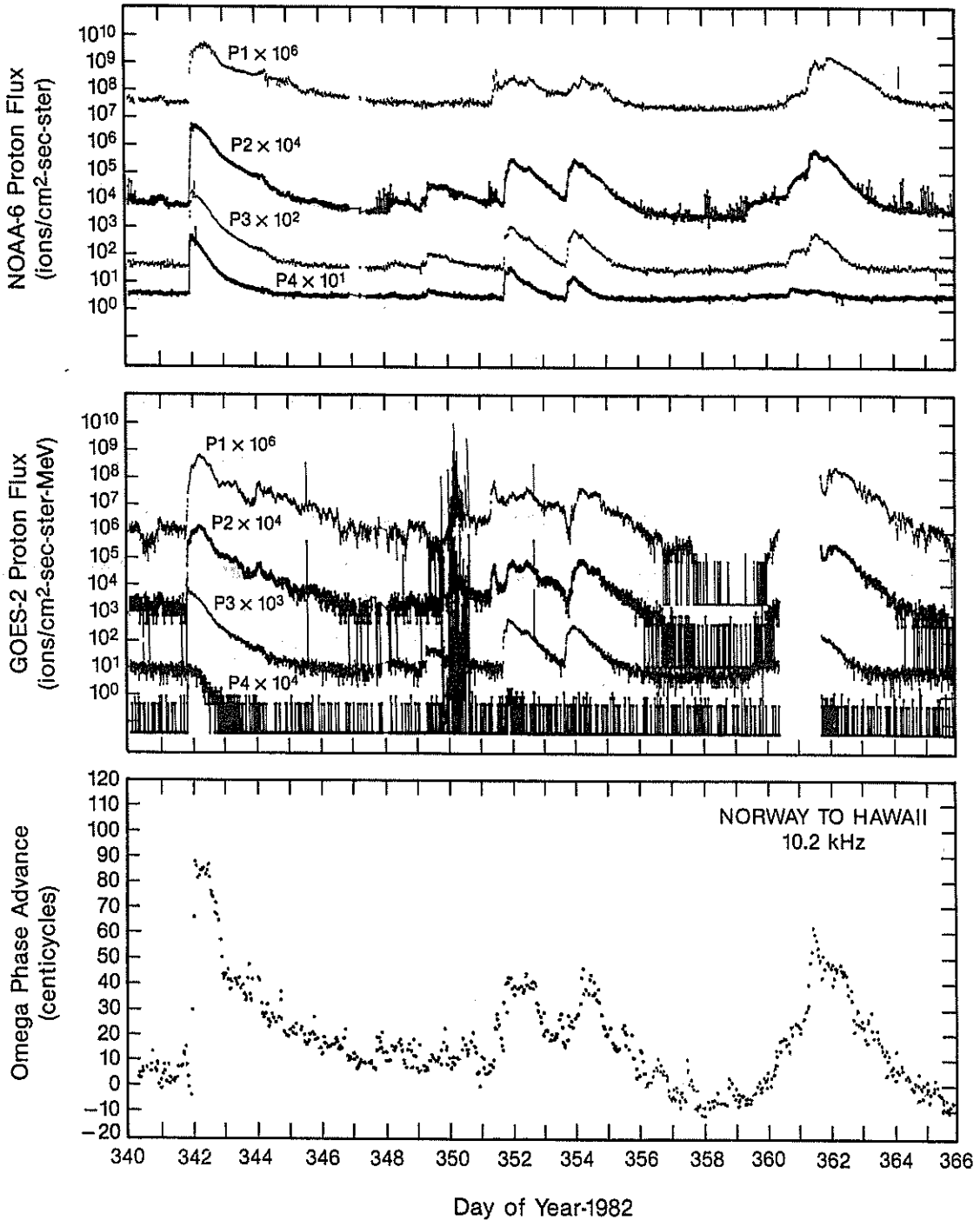

Figure 12 Comparison of Proton Fluxes with H-N Phase Advance
6 December - 31 December, 1982

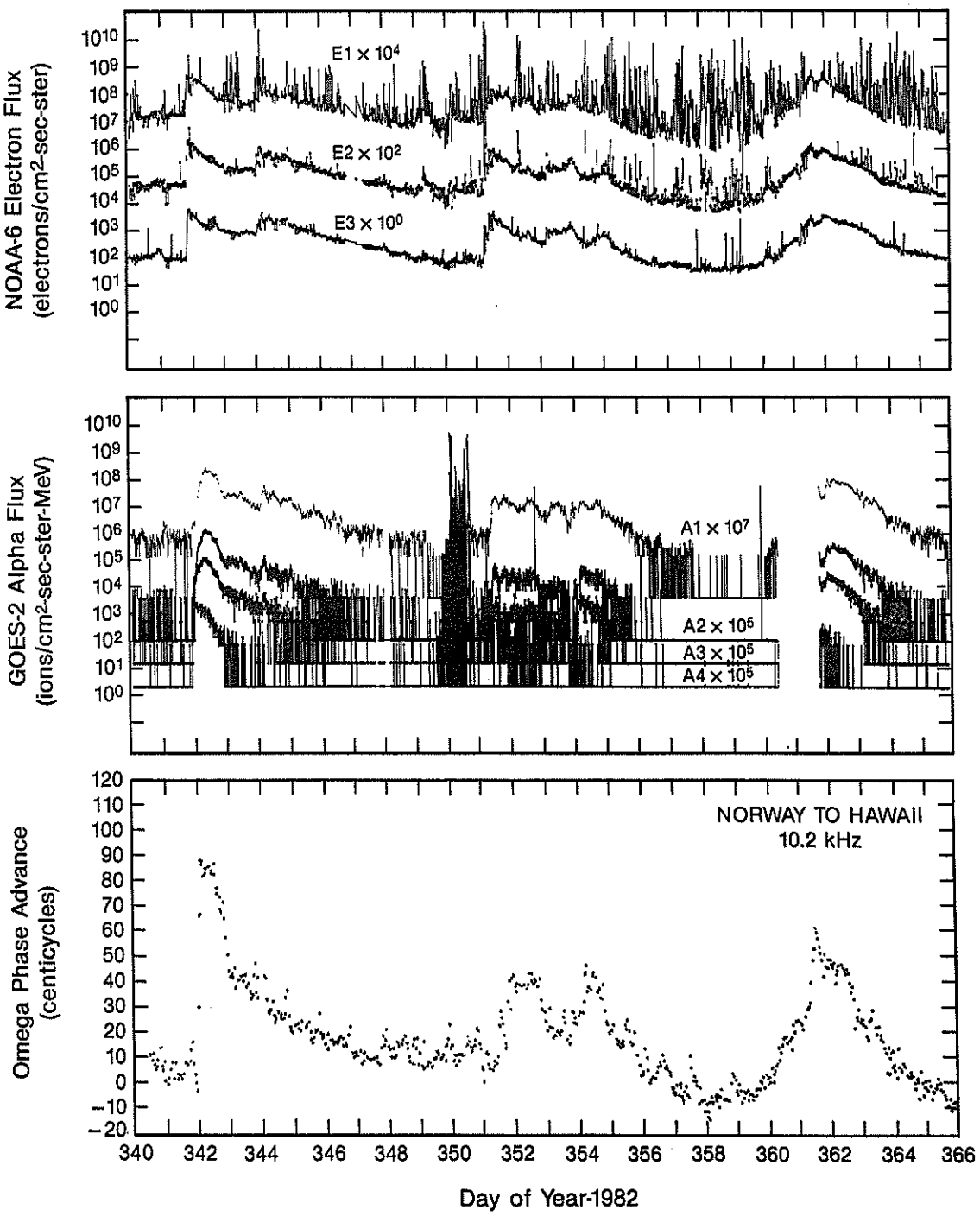

Figure 13 Comparison of Alpha Particle and Electron Fluxes with N-H Phase Advance 6 December - 31 December, 1982

The computer code assumes that the incoming proton (or alpha particle) fluxes at the satellite are 2π - isotropic in the upper hemisphere. Except for a short period at the start of some events, this is generally found to be true. The NOAA-6 detectors measure fluxes in the zenithal direction (those reported here), and also at 90° to the zenith. Sample comparisons of the zenithal and 90° detector count rates during the event periods examined in this study showed differences in these measurements of less than 20%, implying that there were indeed no large anisotropies in the incoming fluxes. The contribution to the ion production rate of particles that mirror below the satellite, and return as upgoing particles, has been neglected. The error introduced by neglecting the small fraction of particles mirroring below the satellite is considered to be less than 10% (Adams and Masely, 1965).

Alpha particles may be treated in the same manner because an alpha particle traversing matter loses energy through ionization at four times the rate of a proton having one-fourth the energy of the alpha particle.

The ion production rate due to the observed precipitating electron fluxes was determined using a computer code in which the passage of electrons through the auroral atmosphere is treated as a diffusive process through the solution of the appropriate diffusion equation (Walt et al., 1968). This procedure takes into account both scattering and energy loss, which are comparable for electron energies of interest here, and also takes into account the effect of the geomagnetic field on the motion of the ionospheric electrons.

The lower panel of Figure 14 presents the results of the calculations for ion production rate over the ionospheric height range of 40 to 110 km, due to the observed fluxes of protons, alpha particles, and electrons measured by

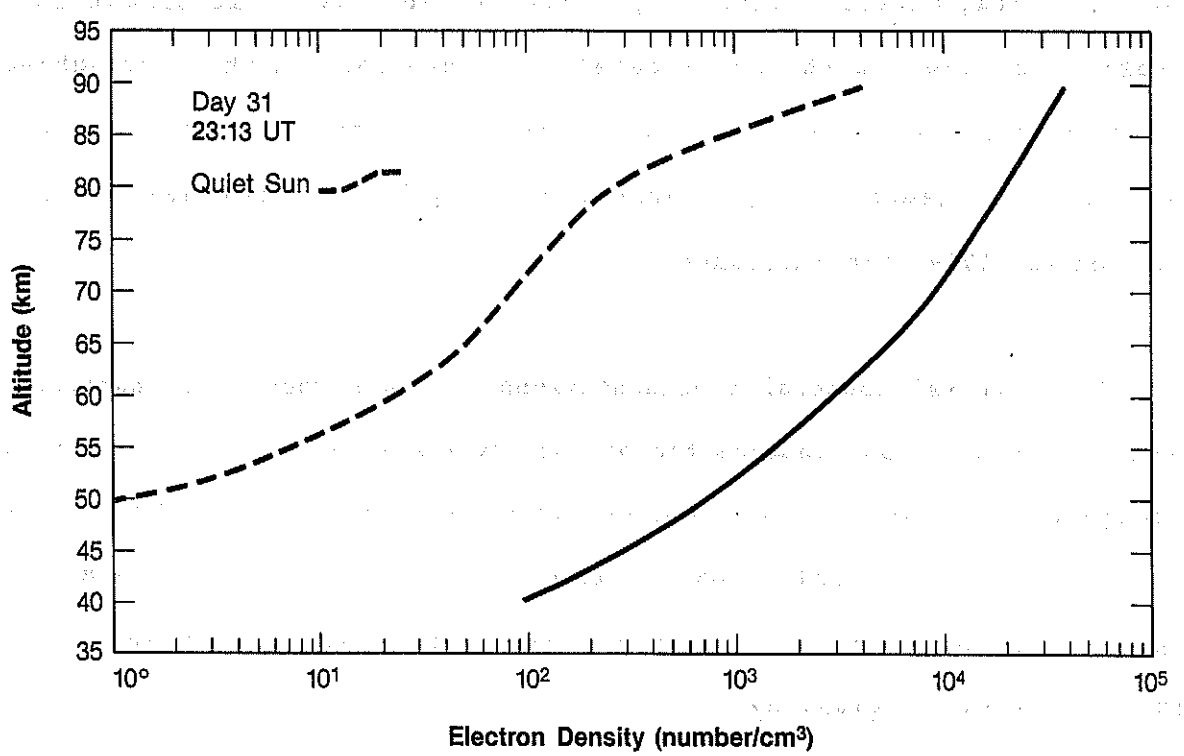

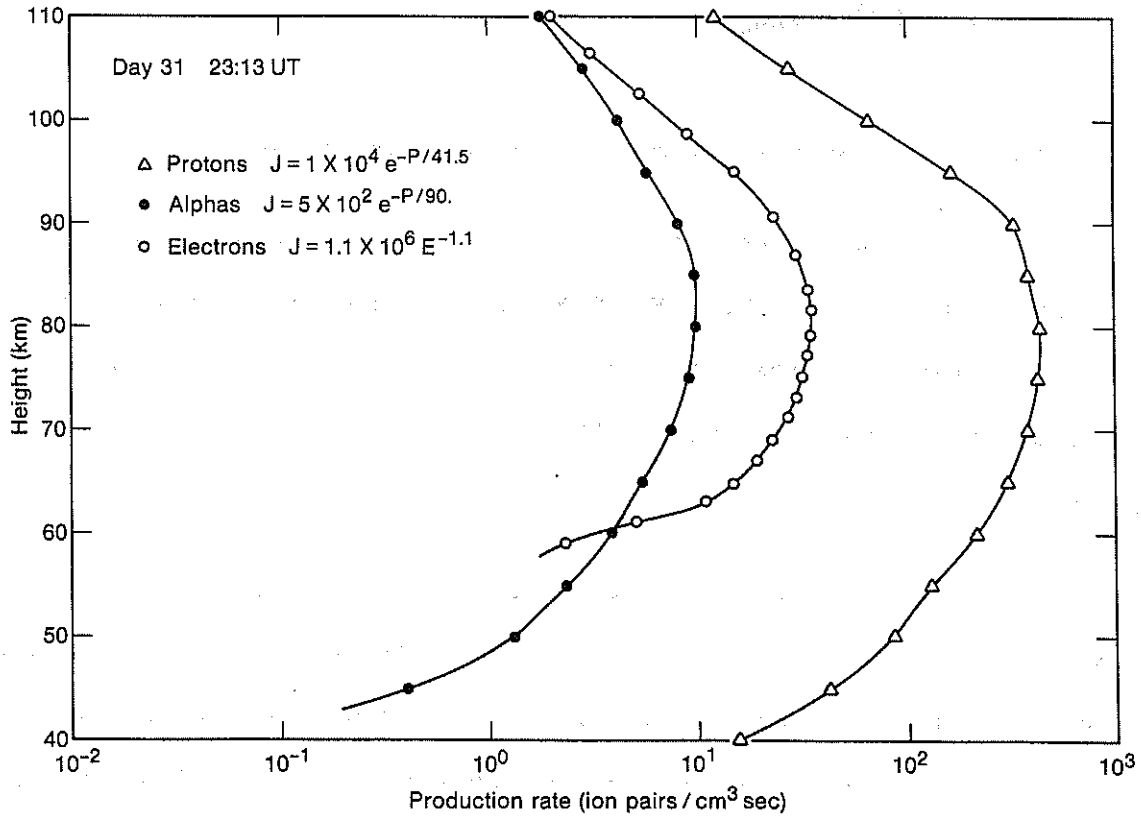

Figure 14 Production Rate and Electron Density Profile - 2313 UT Day 31

the NOAA-6 and GOES-2 satellites at 2313 UT on Day 31 (Jan. 31). The corresponding electron density profile obtained for this production rate profile is shown in the upper panel of Figure 14. In this and subsequent plots of electron density-height profiles, the dotted line curve represents the electron density height profiles for quiet sun periods as given by Hargreaves (1979) for reference.

The integral spectral representations for each species of particle were obtained from a least squares fit of the observational data to a power law in energy in the case of electrons, and as an exponential rigidity spectrum in the case of protons and alpha particles. The relationship between particle energy E in MeV (million electron volts), and particle rigidity P in MV (Million volts) is given by

$$P = \sqrt{E^2 + 2EE_o}$$

where E_o is the rest mass energy of the particle in MeV.

Figure 14 shows that near the time of peak anomalous phase advance (peak proton flux) of the 10.2 kHz H-N signal, the contribution to the ion production rate over the altitude range of interest of both the electron and alpha particle precipitation is 10% or less of that produced by precipitating protons.

Figure 15 shows similar plots of ion production rate and electron density profiles at 1600 UT of Day 42 (11 Feb.). Only an electron contribution is shown, because the proton and alpha particle fluxes had fallen below threshold during this period. As noted earlier, this period (Days 41-44) was the only

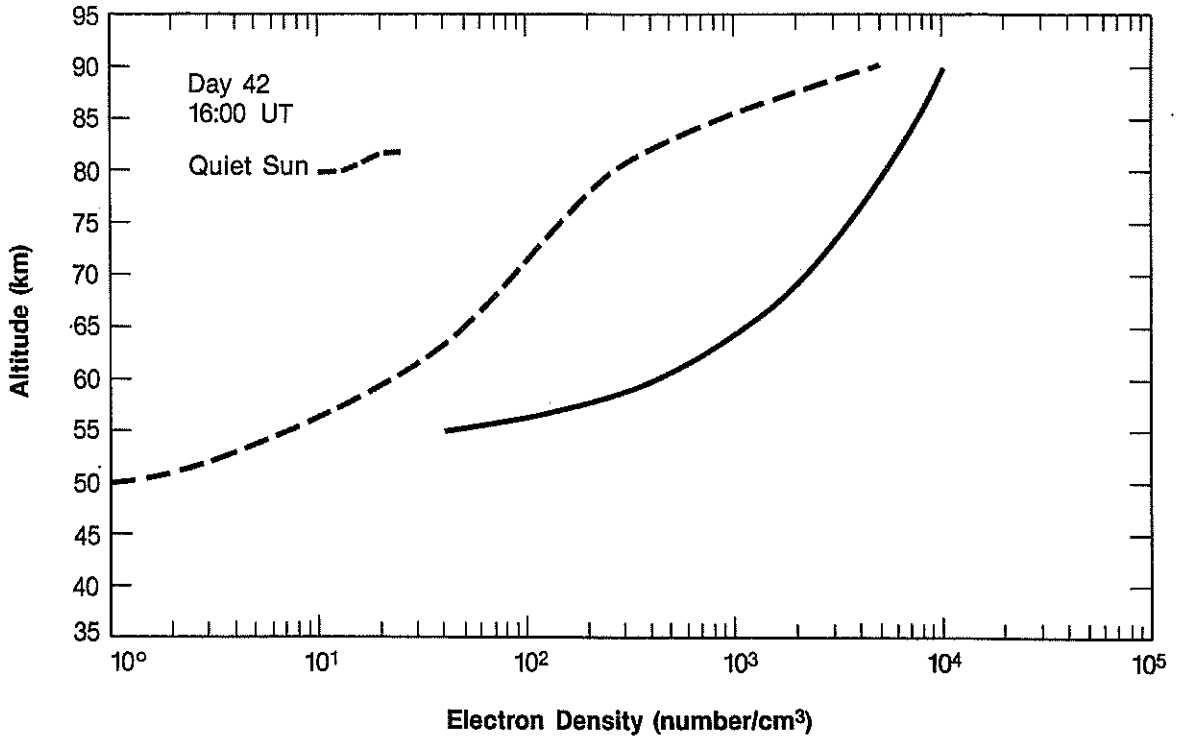

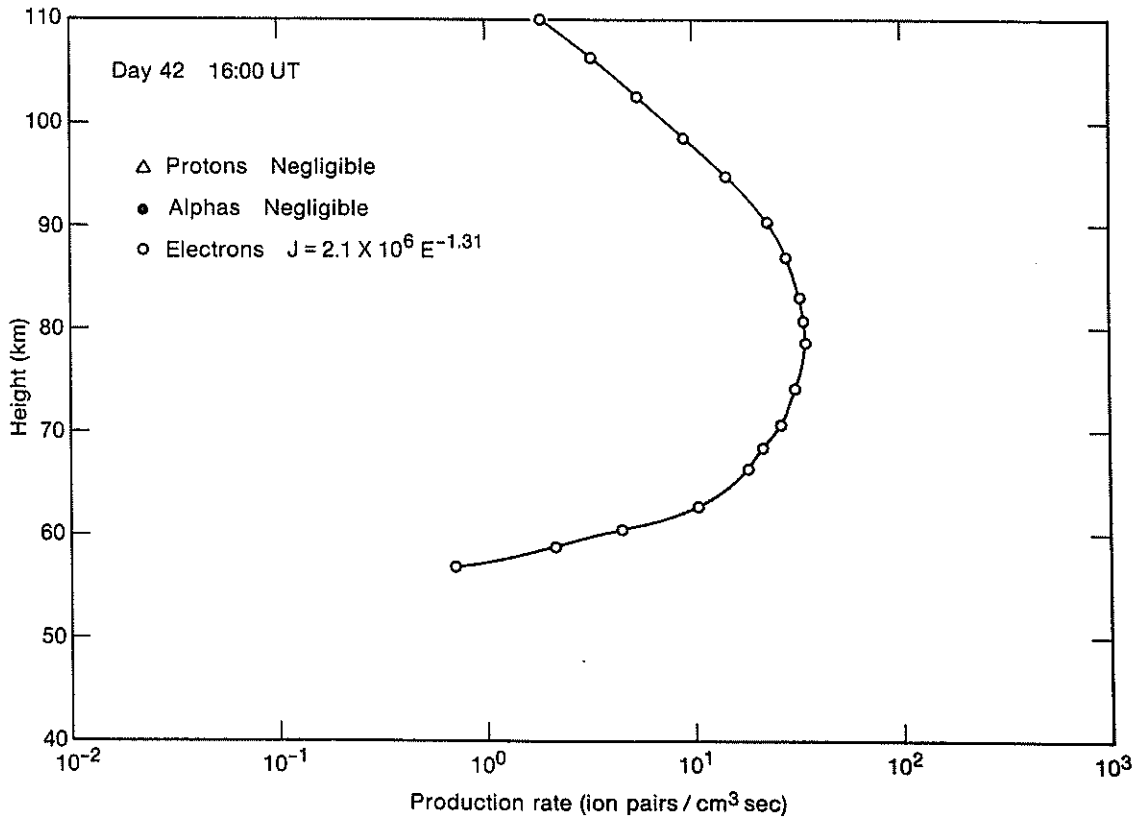

Figure 15 Production Rate and Electron Density Profile - 1600 UT Day 42

one, during the seven solar cosmic ray events examined, that demonstrated an apparent delayed recovery of the 10.2-kHz signal with respect to the principal proton fluxes.

Figures 16 and 17 show corresponding plots of ion production rate and electron density versus altitude for the peak (Day 194 = 13 July) and late phase (Day 199 = 18 July) of the second event examined. At the peak of the event (Fig. 16), the proton-produced ion production rate again exceeds the rates of both the alpha particles and the electrons by a factor of ~10. As in all cases, the height profiles of the proton and the alpha particle-produced ion production are quite similar (similar alpha-proton ratio), while production produced by the precipitating electron fluxes falls rapidly below about 60 to 65 km.

Figure 17 represents the production rate and the resulting electron density profile late in the second event (Day 199 = 18 July). The alpha particle flux had fallen below background and is shown as negligible. At high altitudes (height >78 km), the electron-produced ion production exceeds that due to protons, becoming equal at about 78 km. Below 78 km, the electron-produced production rapidly falls to a negligible fraction of that due to the precipitating protons.

Figures 18, 19, and 20 present corresponding representative plots of ion production rates and electron density profiles for the peak event periods of Day 204 (23 July), Day 342 (8 Dec.), and Day 362 (28 Dec.). For all event periods examined, the protons provided the dominant ($\geq$90%) ion production source, at least when their fluxes were above instrument threshold, with the possible exception of the period during Day 42 (11 Feb.) when both the proton and alpha particle fluxes had fallen to below instrumental threshold.

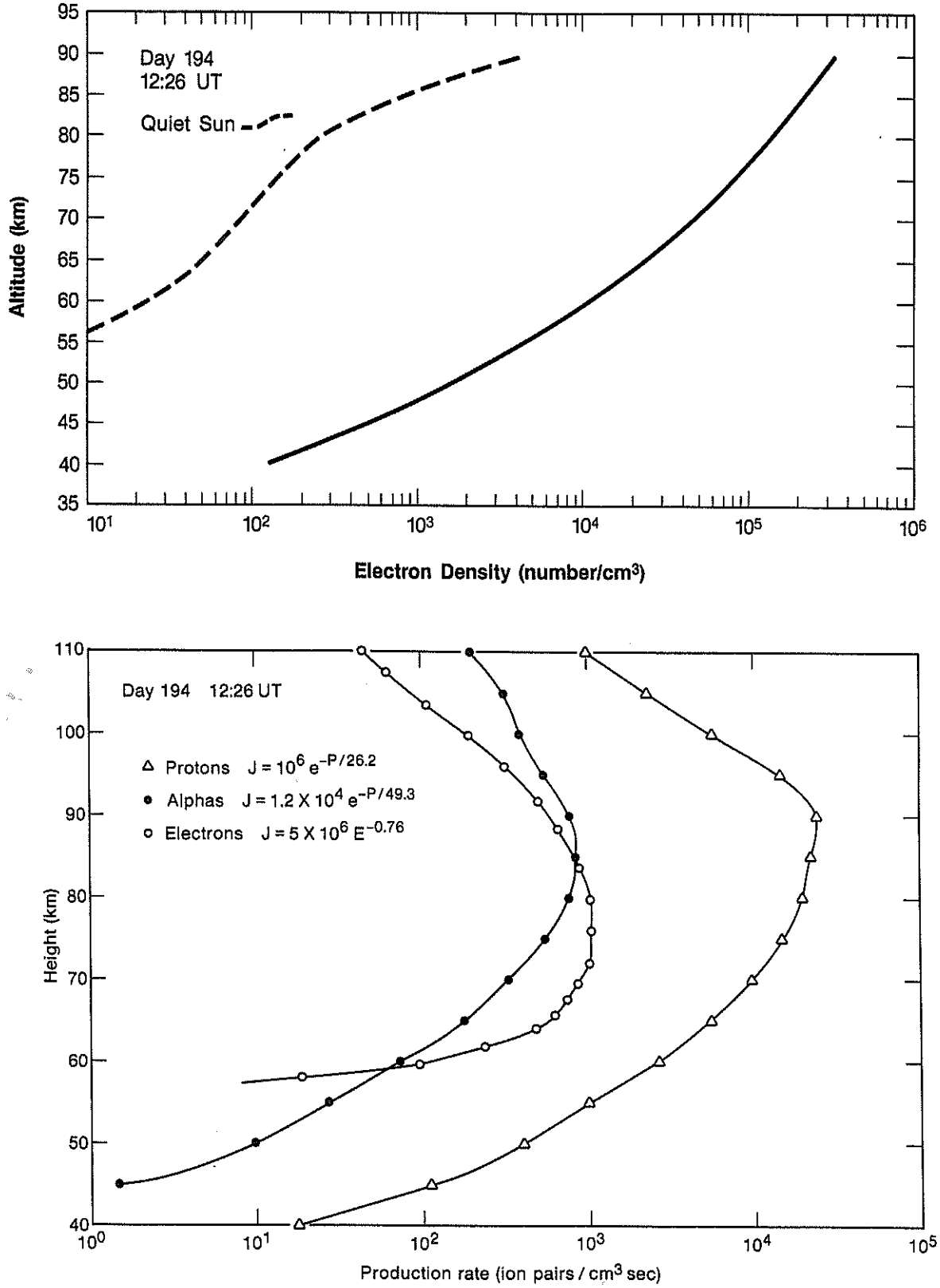

Figure 16 Production Rate and Electron Density Profile - 1226 UT Day 194

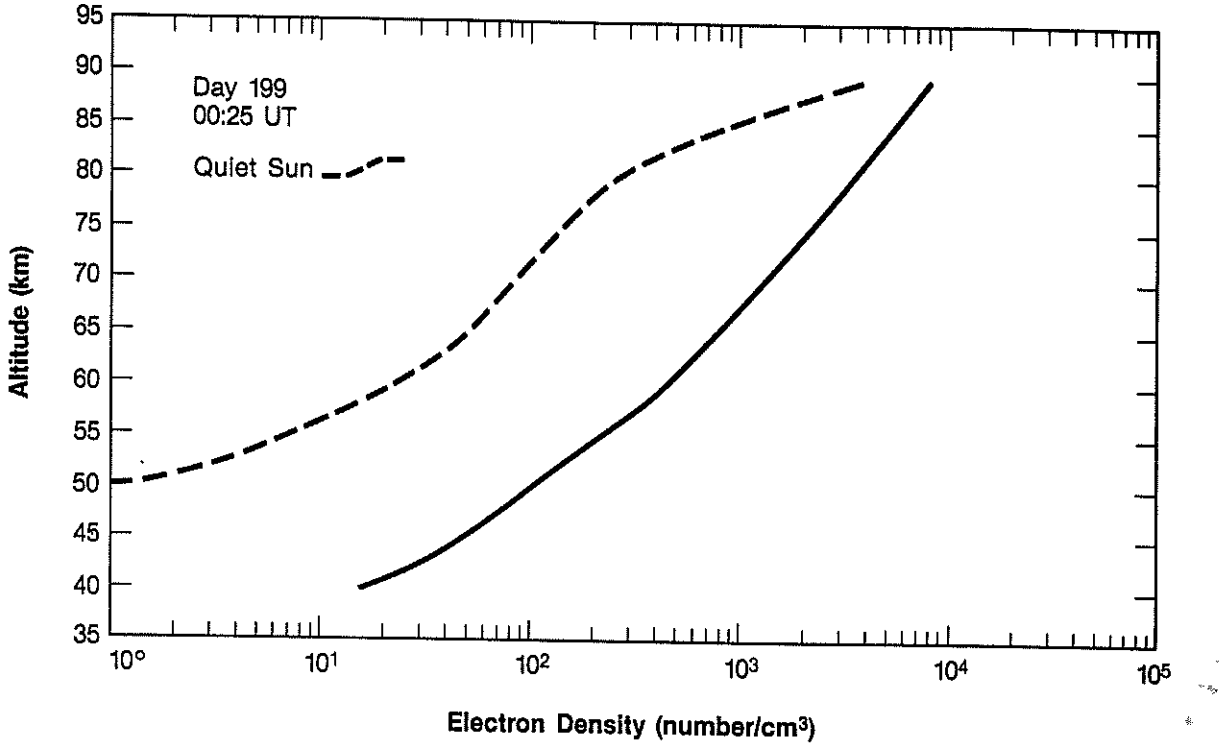

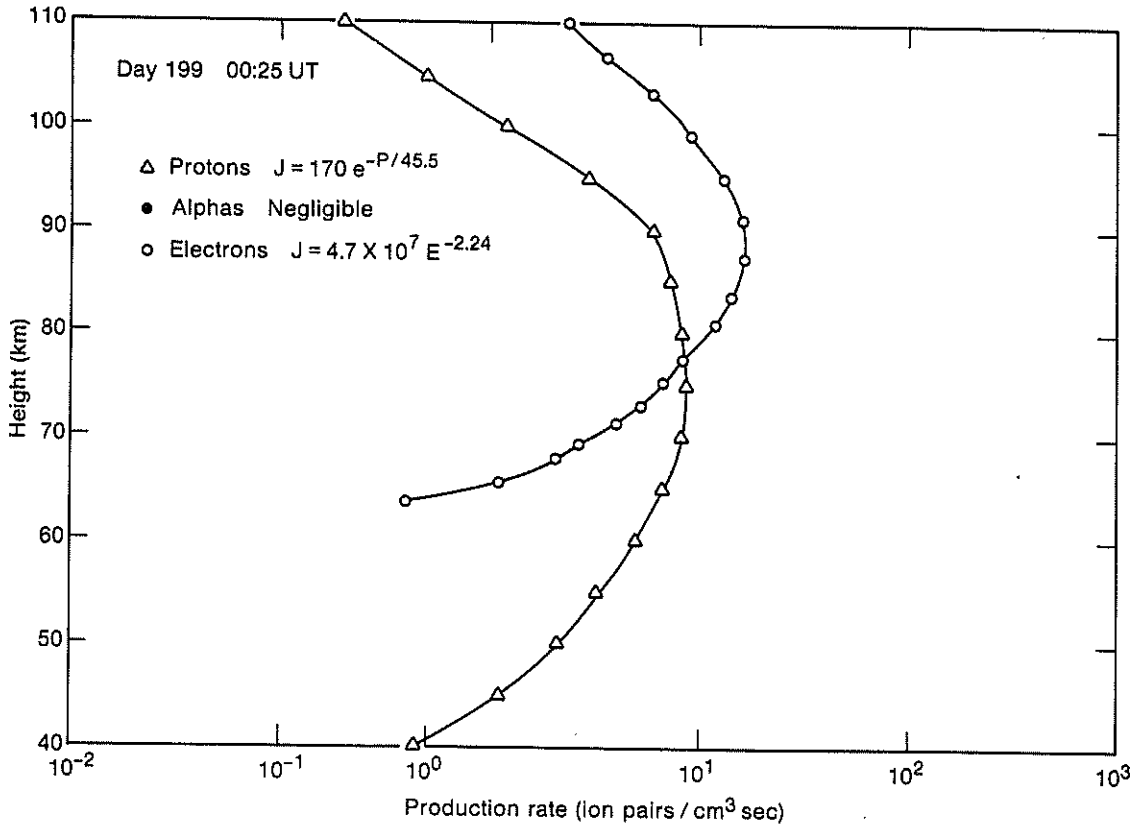

Figure 17 Production Rate and Electron Density Profile - 0025 UT Day 199

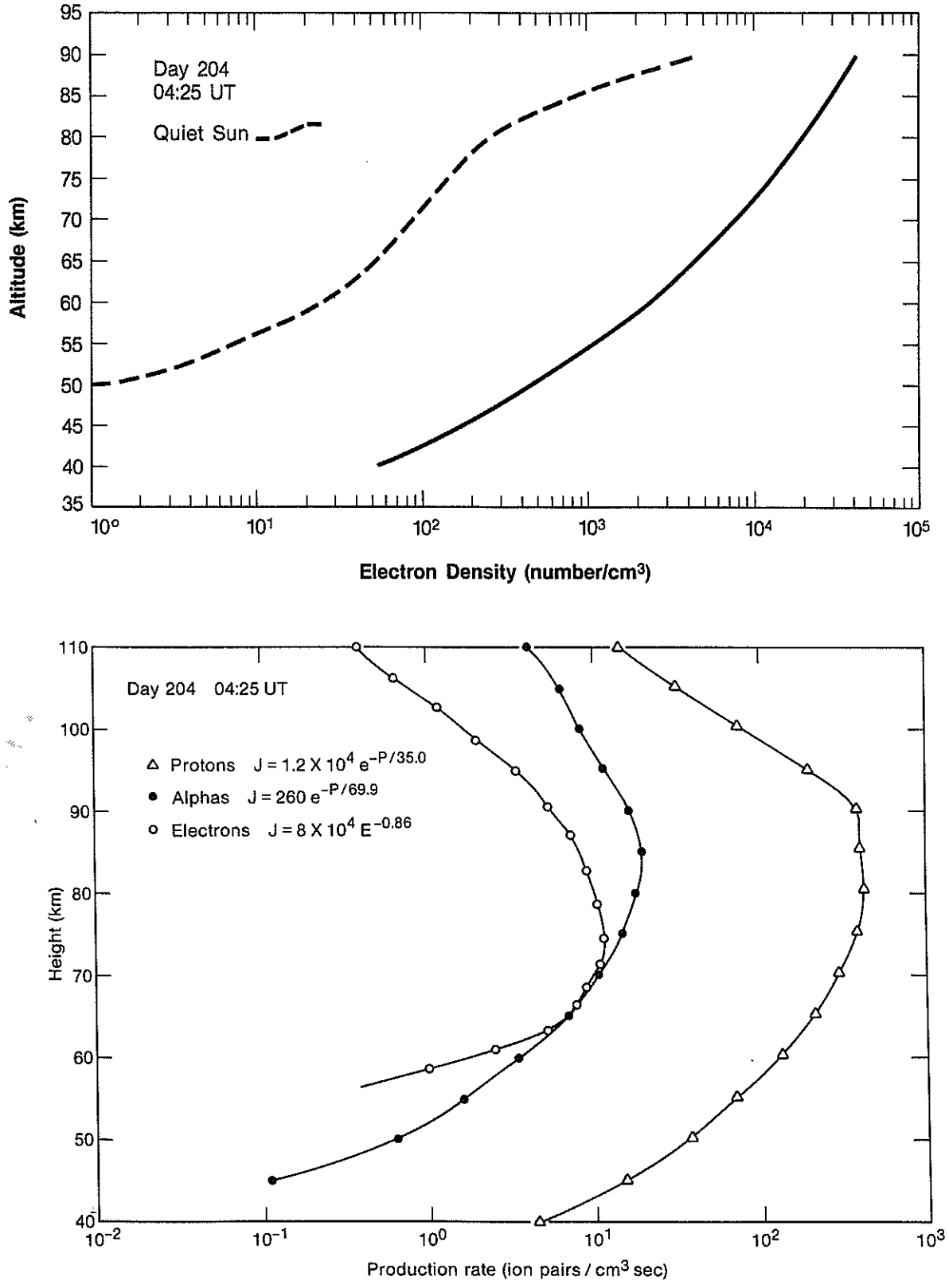

Figure 18 Production Rate and Electron Density Profile - 0424 UT Day 204

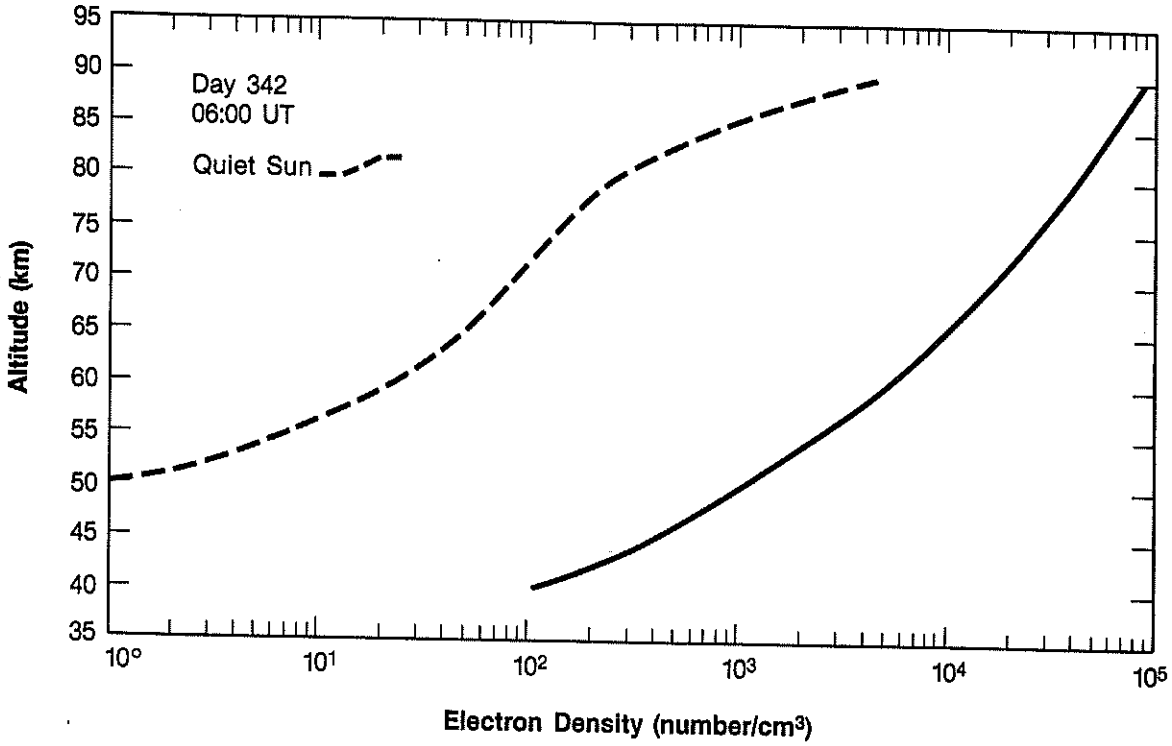

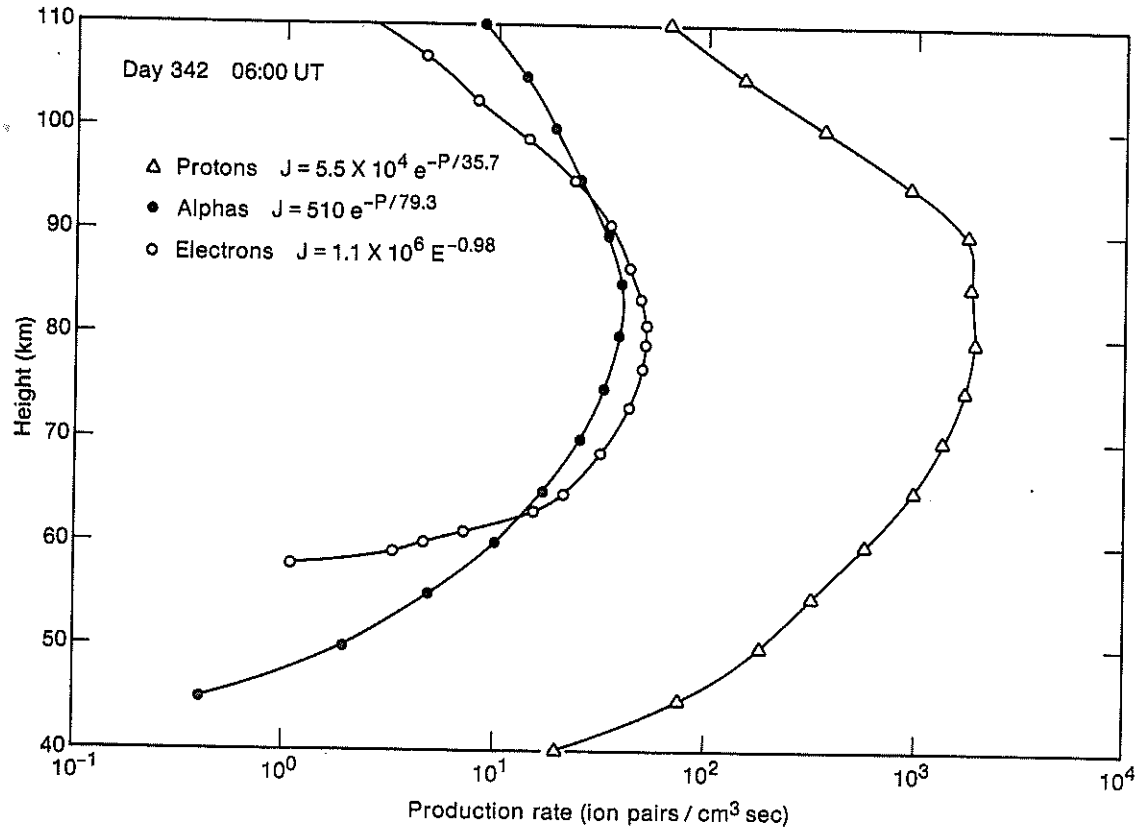

Figure 19 Production Rate and Electron Density Profile - 0600 UT Day 342

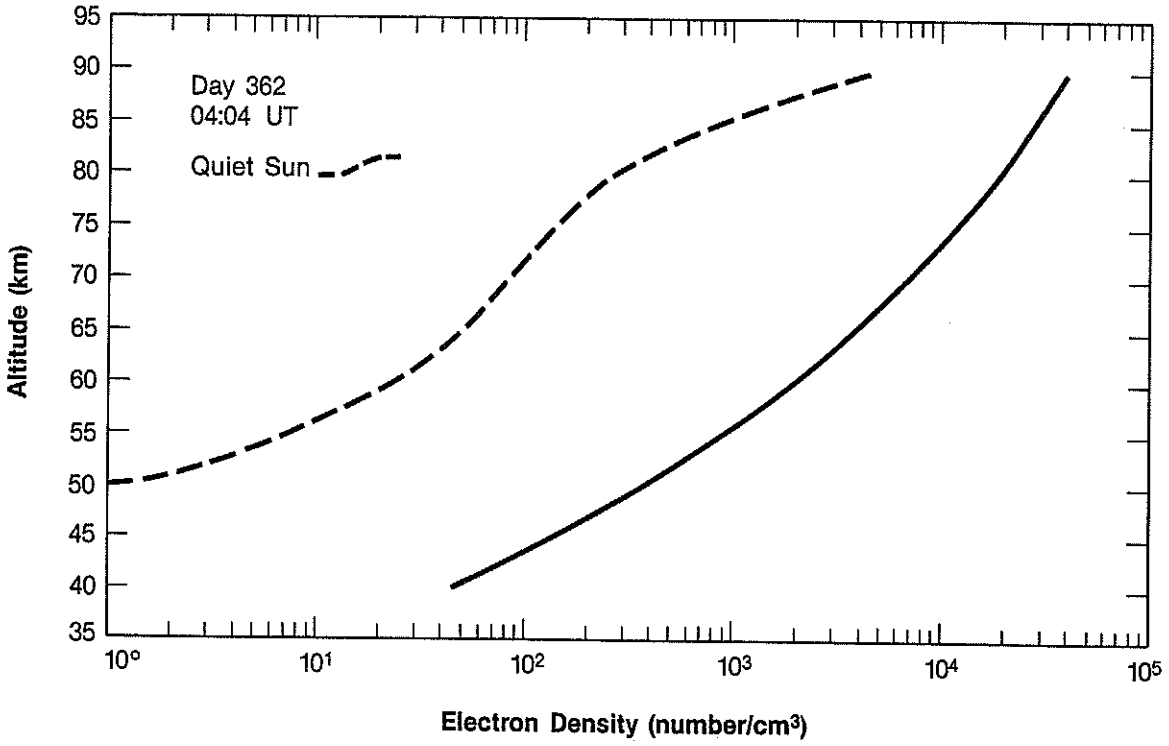

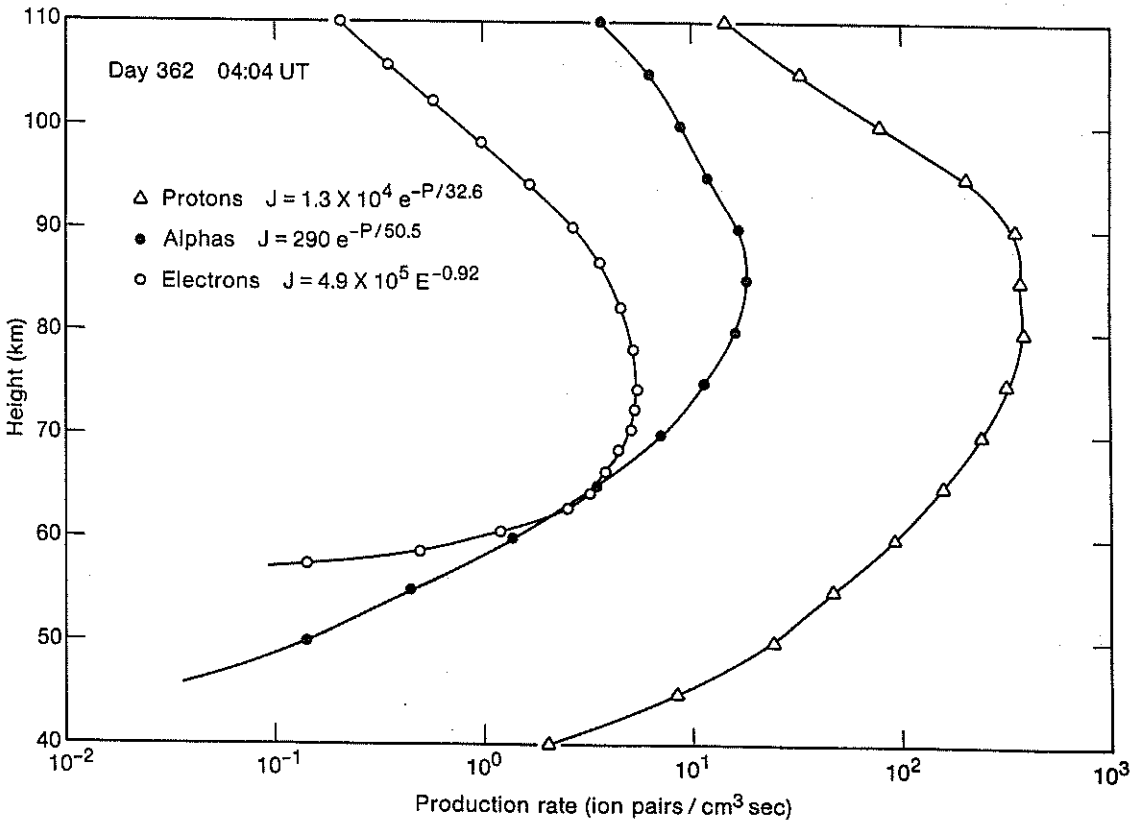

Figure 20 Production Rate and Electron Density Profile - 0404 UT Day 362

5. DISCUSSION

The seven solar cosmic ray events examined, which occurred during three extended periods of 1982, represented a sampling of most of the major events in which the anomalous phase advance observed on the Hawaii-Norway (H-N), 10.2-kHz signal path exceeded 40 centicycles, and included events occurring in both winter and summer. Path illumination conditions are quite different for the two seasons. The path is almost fully and continually illuminated in summer, but in winter there is a substantial diurnal variation in the percentage of path illuminated.

Argo (1975) has indicated a strong dependence of the OMEGA phase advance on the fraction of the path that is sunlit. Further, theoretical (Davies, 1965) and experimental (Westerlund et al., 1969) studies have indicated that the OMEGA phase advance is proportional to the log log of the integral flux above some nominal threshold like 25 MeV. Despite this, the time profiles of the precipitating proton and alpha particle fluxes observed by the NOAA-6 and GOES-2 satellite during seven solar cosmic ray events occurring in 1982 appear to be almost congruent to the phase advance of the 10.2-kHz OMEGA H-N path. This is especially evident for the GOES-2 P1 (6 MeV) channel in Figures 9 through 13. The only apparent exception to this observation is the period around Day 42, during which Figure 15 indicates that the electron density was enhanced at heights above about 54 km from quiet sun levels. However, it seems somewhat paradoxical that the electron fluxes were monotonically increasing during this day, while the OMEGA phase advance was observed to generally decrease.

As a heuristic exercise, a least squares fit of the logarithm of the GOES-2 P1 proton flux versus the 10.2-kHz H-N phase advance in centicycles was

performed for the rise to maximum of the 13 July event. The resulting parameters yielded the following expression for the phase advance of the H-N path, A, in centicycles, in terms of the 6 MeV GOES-2 differential particle flux J:

$$A = 8.24 \ln (8.7 J) \quad (1)$$

In Figure 21, the time profiles of the observed 6-MeV differential flux are plotted as a solid line for all the examined event periods. The phase advances calculated for each GOES-2 6-MeV differential flux measurement from eq. 1 are superimposed. The correspondence between the observed value and the calculated phase advance for the period Day 192 to Day 208 is remarkably close. There is evidence for both a semidiurnal and diurnal variation amounting to some ± 10 centicycles. As noted earlier, the H-N path is almost fully illuminated, but from the analysis of Argo (1975) one would still expect a small diurnal variation because of the diurnal change in fractional path illumination. One would also expect a semidiurnal variation because of the oval shape of the polar cap (auroral oval) and the resulting polar path length change. From an operational point of view, however, the calculated values very well represent the time profile of the events throughout the 20-day period.

The same calculation (eq. 1) was applied to the other two event periods with surprisingly good results. The top panel of Figure 21 shows the comparison for the first observation period of 30 January (Day 30) - 12 February 1982. Although there was a substantial data gap from Day 33 to 38, the general time profile is well represented by the calculated values, which are uniformly about 15 centicycles low. Clearly a least squares fit of the phase advance to the logarithm of the 6-MeV flux based on the start to peak-

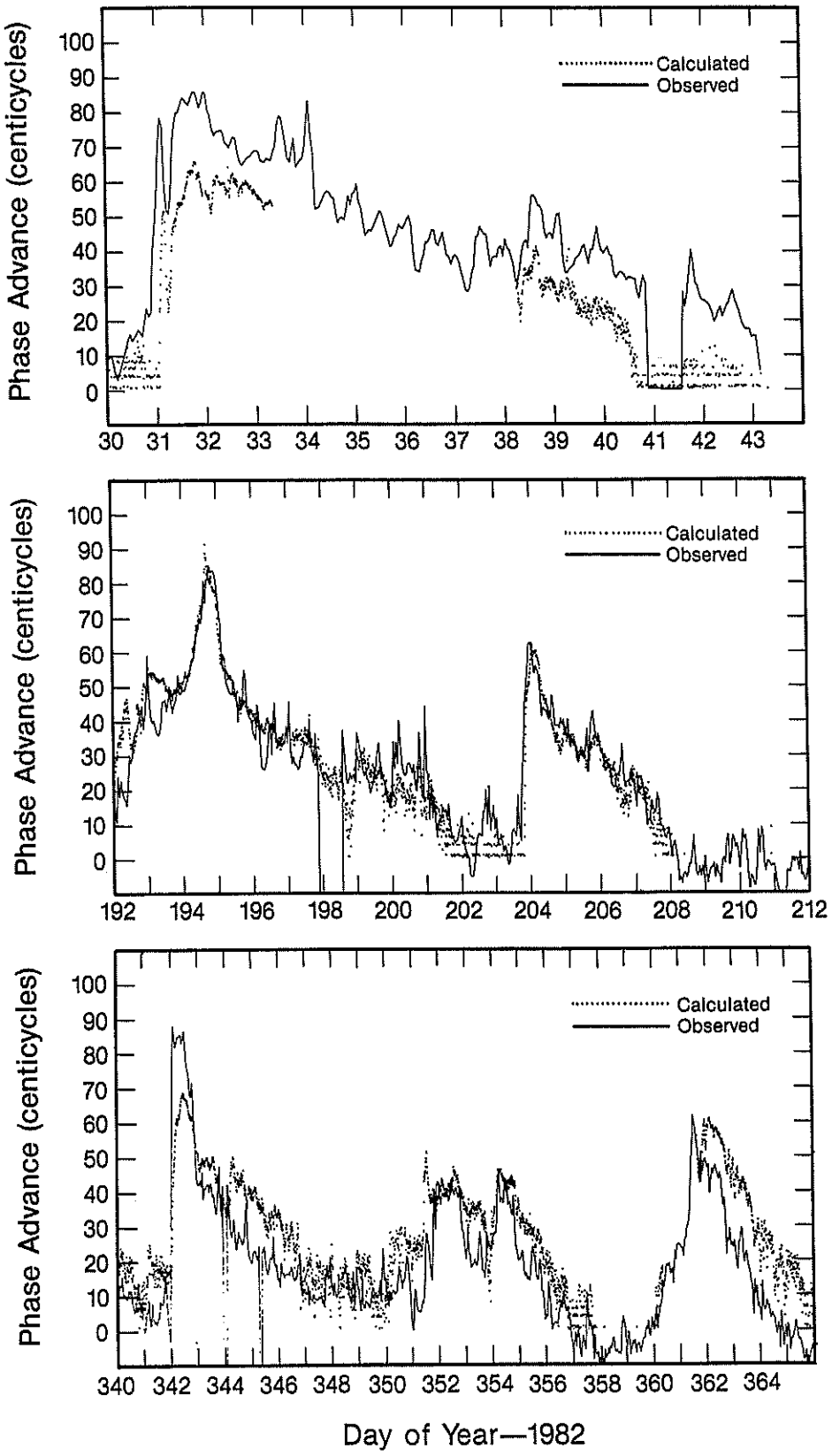

Figure 21 Comparison of Observed and Calculated Phase Advances

time data of this event would produce, again, a relatively good fit, including even the period from Day 41 to 43, during which an apparent delayed recovery (as interpreted from the initial data comparisons) was observed (Fig. 9). Again a semidiurnal and diurnal variation are evident (in fact, somewhat more pronounced than for the summertime events), as might be expected.

Finally, the lower panel of Figure 21 presents the comparison of the phase advance calculated with eq. (1) and that observed during the third event period. Again, the general agreement of the calculated and observed phase advance is quite good. However, the departures are not uniformly systematic over the observation period; rather, there are discrete relative level changes. The calculated values are low during the peak day (Day 342), high during Days 344-346, comparable through the start of the phase advance data gap (Day 358), and high again from Day 362 to the end of the event. These changes seem not to be related to corresponding changes in the alpha-proton ratios, or to the electron-proton ratios observed in the particle data.

This suggests that such a least squares fit of the operationally available 6-MeV geostationary fluxes to the observed anomalous phase advances be made for the paths of interest. Further study would then establish the utility of the resulting algorithms in projecting the OMEGA phase advance from current measurements of geostationary 6-MeV fluxes of protons.

It should be mentioned here that the phase anomalies discussed in this report are not the only ones that were found. The anomalies presented here were chosen because the periods were of special interest to the OMEGA system, because simultaneous particle flux data were available or because the phase data were available at the time of investigation or were of particularly high

quality.

6. CONCLUSION

The event periods studied indicate that the time profiles of the 10.2-kHz OMEGA Hawaii-to-Norway path are very similar to the time profiles of the 6-MeV differential proton flux as observed by the GOES-2 satellite instrumentation.

There is no compelling indication of the presence of unusual ionospheric chemical processes of importance to the response of the OMEGA signal to precipitation solar particle radiations. There is of course clear evidence of diurnal variations relating to changing path illumination and to polar cap shape factors.

The ability of a single simple algorithm, based on the observed 6-MeV differential proton fluxes, to reasonably represent the observed H-N anomalous phase advance, suggests that operational assessments of OMEGA PCA response be based on the 6-MeV differential flux rather than the published integral fluxes above some arbitrary threshold.

IV Acknowledgments

The authors wish to acknowledge the support provided for this study by the U.S. Coast Guard OMEGA Navigation System Operational Detail (ONSOD) through order number Z7099-3-03714. In addition, thanks are due to Mr. Peter B. Morris of the ONSOD for making the OMEGA phase data available, and for useful discussion.

V. References

Adams, G. W., and A. J. Masely, Production Rates and Electron Densities in the Lower Ionosphere due to Solar Cosmic Rays, J. Atmos. Terr. Phys., 27, 289-298, 1965.

Argo, P. E., Modeling OMEGA PCA Phase Advances, Naval Elec. Lab. Center, NELC/TR 1950, San Diego, 1975.

Chilton, C. J., and J. H. Crary, ULF Observations of Nighttime D-region Ionization Enhancement by the Scorpius XR-1 X-ray Source, Radio Sci. J. Res., 6 (7), 699-708, 1971.

Crombie, D. C., Periodic Fading of VLF Signals Received over Long Paths at Sunrise and Sunset, Radio Sci. J. Res., NBS 68D(1), 27-34, 1964.

Davies, K., Ionospheric Radio Propagation, National Bureau of Standards Monograph 80, 1965.

Firor, J., Cosmic Ray Intensity-Time Variations and their Origin., Phys. Rev., 94, 1017, 1954.

Hargreaves, J.K., The Upper Atmosphere and Solar-Terrestrial Relations, Van Nastrand Rheinhold, 1979.

Lanzerotti, L. J., Penetration of Solar Protons and Alphas to the Geomagnetic Equator, Phys. Rev. Letters, 21, 929, 1968.

Piazzo, L. Rizzo, P. Kaufman, and P. Ramirey Pardo, VLF Ionosonde and Long Distance Propagation Anomalies produced by Cen X-4 X-ray Burst in May 1979, J. Atmos. Terr. Phys., 45 (2/3), 121-125, 1983.

Rossi, B., and S. Olbert, Introduction to the Physics of Space, McGraw-Hill, 1979.

Swanson, E. R., OMEGA Conf. Proc., Brussels, Belgium, 21-25 September 1981, AGARD-CP-305, 36/1-16, 1981.

Westerlund, S., F. H. Reder, and C. Abom, Effects of Polar Cap Absorption Events on VLF Transmissions, Planet. Space. Sci., 17, 1329-1374, 1969.

Walt, M., W. M. MacDonald, and W. E. Francis, Penetration of Auroral Electrons into the Atmosphere, Physics of the Magnetosphere, R. L. Carovillano, J. F. McClug, H. R. Radoski, (eds.), D. Reidel , 534-555, 1968.

Appendix

DAY OF THE YEAR CALENDAR

(FOR NONLEAP YEARS)

DAY	JAN	FEB	MAR	APR	MAY	JUN	JUL	AUG	SEP	OCT	NOV	DEC	DAY
1	001	032	060	091	121	152	182	213	244	274	305	335	1
2	002	033	061	092	122	153	183	214	245	275	306	336	2
3	003	034	062	093	123	154	184	215	246	276	307	337	3
4	004	035	063	094	124	155	185	216	247	277	308	338	4
5	005	036	064	095	125	156	186	217	248	278	309	339	5
6	006	037	065	096	126	157	187	218	249	279	310	340	6
7	007	038	066	097	127	158	188	219	250	280	311	341	7
8	008	039	067	098	128	159	189	220	251	281	312	342	8
9	009	040	068	099	129	160	190	221	252	282	313	343	9
10	010	041	069	100	130	161	191	222	253	283	314	344	10
11	011	042	070	101	131	162	192	223	254	284	315	345	11
12	012	043	071	102	132	163	193	224	255	285	316	346	12
13	013	044	072	103	133	164	194	225	256	286	317	347	13
14	014	045	073	104	134	165	195	226	257	287	318	348	14
15	015	046	074	105	135	166	196	227	258	288	319	349	15
16	016	047	075	106	136	167	197	228	259	289	320	350	16
17	017	048	076	107	137	168	198	229	260	290	321	351	17
18	018	049	077	108	138	169	199	230	261	291	322	352	18
19	019	050	078	109	139	170	200	231	262	292	323	353	19
20	020	051	079	110	140	171	201	232	263	293	324	354	20
21	021	052	080	111	141	172	202	233	264	294	325	355	21
22	022	053	081	112	142	173	203	234	265	295	326	356	22
23	023	054	082	113	143	174	204	235	266	296	327	357	23
24	024	055	083	114	144	175	205	236	267	297	328	358	24
25	025	056	084	115	145	176	206	237	268	298	329	359	25
26	026	057	085	116	146	177	207	238	269	299	330	360	26
27	027	058	086	117	147	178	208	239	270	300	331	361	27
28	028	059	087	118	148	179	209	240	271	301	332	362	28
29	029		088	119	149	180	210	241	272	302	333	363	29
30	030		089	120	150	181	211	242	273	303	334	364	30
31	031		090		151		212	243		304		365	31
DAY	JAN	FEB	MAR	APR	MAY	JUN	JUL	AUG	SEP	OCT	NOV	DEC	DAY

(FOR NONLEAP YEARS)